Exploring long-range cooperativity in the 20S proteasome core particle from *Thermoplasma acidophilum* using methyl-TROSY–based NMR

Enrico Rennella[a,b,c,1], Rui Huang[a,b,c], Zanlin Yu[d], and Lewis E. Kay[a,b,c,e,1]

[a]Department of Molecular Genetics, The University of Toronto, Toronto, ON M5S1A8, Canada; [b]Department of Biochemistry, The University of Toronto, Toronto, ON M5S1A8, Canada; [c]Department of Chemistry, The University of Toronto, Toronto, ON M5S1A8, Canada; [d]Department of Biochemistry and Biophysics, University of California, San Francisco, CA 94143; and [e]Program in Molecular Medicine, The Hospital for Sick Children, Toronto, ON M5G1X8, Canada

Edited by Kylie J. Walters, National Cancer Institute, NIH, Bethesda, MD, and accepted by Editorial Board Member Michael F. Summers January 21, 2020 (received for review November 26, 2019)

The 20S core particle (CP) proteasome is a molecular assembly catalyzing the degradation of misfolded proteins or proteins no longer required for function. It is composed of four stacked heptameric rings that form a barrel-like structure, sequestering proteolytic sites inside its lumen. Proteasome function is regulated by gates derived from the termini of α-rings and through binding of regulatory particles (RPs) to one or both ends of the barrel. The CP is dynamic, with an extensive allosteric pathway extending from one end of the molecule to catalytic sites in its center. Here, using methyl-transverse relaxation optimized spectroscopy (TROSY)-based NMR optimized for studies of high–molecular-weight complexes, we evaluate whether the pathway extends over the entire 150-Å length of the molecule. By exploiting a number of different labeling schemes, the two halves of the molecule can be distinguished, so that the effects of 11S RP binding, or the introduction of gate or allosteric pathway mutations at one end of the barrel can be evaluated at the distal end. Our results establish that while 11S binding and the introduction of key mutations affect each half of the CP allosterically, they do not further couple opposite ends of the molecule. This may have implications for the function of so-called "hybrid" proteasomes where each end of the CP is bound with a different regulator, allowing the CP to be responsive to both RPs simultaneously. The methodology presented introduces a general NMR strategy for dissecting pathways of communication in homo-oligomeric molecular machines.

allostery | proteasome gates | *in*/*out* gating equilibrium | 11S regulatory particle

The proteasome plays a critical role in cellular homeostasis by degrading proteins that are aberrantly folded or that are no longer required for function (1–6). It is composed of a 20S core particle (CP) consisting of four stacked heptameric rings that sequester proteolytic sites inside the core of a barrel-like structure and often additional large complexes, such as the 19S regulatory particle (RP) (7–9), that are bound to one or both ends of the barrel (10, 11) so as to control entry of substrates into the 20S CP for degradation. Each of the pair of outer and inner rings of the 20S CP is made up of seven distinct α- and β-subunits, respectively, in the case of eukaryotic CPs (12–14), but for the simpler archaeal versions, such as the 20S CP from *Thermoplasma acidophilum* studied here, there is often only one type of α- and β-subunit (15–17) so that the 20S CP ring in this case has a simple $\alpha_7\beta_7\beta_7\alpha_7$ architecture (Fig. 1*A*).

Substrate entry into the 20S CP occurs through 13-Å-diameter pores at either end of the symmetric molecule (13, 18). These pores, in turn, are gated via the N-terminal 10 to 15 residues from the α-subunits preventing the indiscriminate passage of substrates into the lumen of the proteasome (13, 19). In the case of the 20S CP from *T. acidophilum*, the gates have a high propensity (~95%) to adopt a conformation in which they lie inside the proteasome cavity (referred to as the *in* conformation) (19, 20), but no more than two gates can be accommodated inside the wild-type (WT) 20S *T. acidophilum* CP at one time due to steric hindrance (21), leaving the other five gates exterior to the CP (*out* conformation). These gates are intrinsically disordered and dynamic over a wide range of timescales. For example, they have large amplitude picosecond-to-nanosecond timescale motions (19), undergo significant conformational heterogeneity on the millisecond timescale as established by relaxation dispersion NMR studies (22), and exchange between *in* and *out* conformations on the seconds timescale (19).

A number of different 20S CP regulators of activity have been identified. These include the hexameric 19S RP in eukaryotes that recognizes ubiquitin-tagged substrates and unfolds and threads them through the CP pore for degradation in an ATP-dependent manner (7, 9, 23–26), the corresponding prokaryotic unfoldases such as PAN (27–30) or VAT (28, 29) that also require ATP, and ATP-independent regulators that include the single polypeptide chain PA200 (31, 32) or its yeast ortholog Blm10 (33–35), and the heptameric 11S activators (36–44). Notably, despite their very different architectures, these RPs all use a common mode of interaction with the 20S CP whereby the C-terminal carboxylic group from monomeric RPs (Blm10/PA200) or from at least one of the

Significance

The proteasome is a molecular machine that plays a key role in maintaining the healthy function of cells through eliminating protein molecules that are no longer required or that are damaged. Proteasome function is, in part, regulated through the binding of other protein components that turn on pathways of communication between the sites of binding and distal regions of the proteasome that are responsible for its catalytic activity. Understanding how information is communicated between far-removed sites in the proteasome, and the extent of the pathway of communication, is a key first step in the design of molecules that can regulate its activity, with potentially important implications in the fight against certain cancers and neurodegenerative diseases.

Author contributions: E.R., R.H., Z.Y., and L.E.K. designed research; E.R., R.H., and L.E.K. performed research; E.R. and L.E.K. analyzed data; and E.R. and L.E.K. wrote the paper.

The authors declare no competing interest.

This article is a PNAS Direct Submission. K.J.W. is a guest editor invited by the Editorial Board.

See online for related content such as Commentaries.

[1]To whom correspondence may be addressed. Email: rennella@pound.med.utoronto.ca or kay@pound.med.utoronto.ca.

This article contains supporting information online at https://www.pnas.org/lookup/suppl/doi:10.1073/pnas.1920770117/-/DCSupplemental.

First published February 24, 2020.

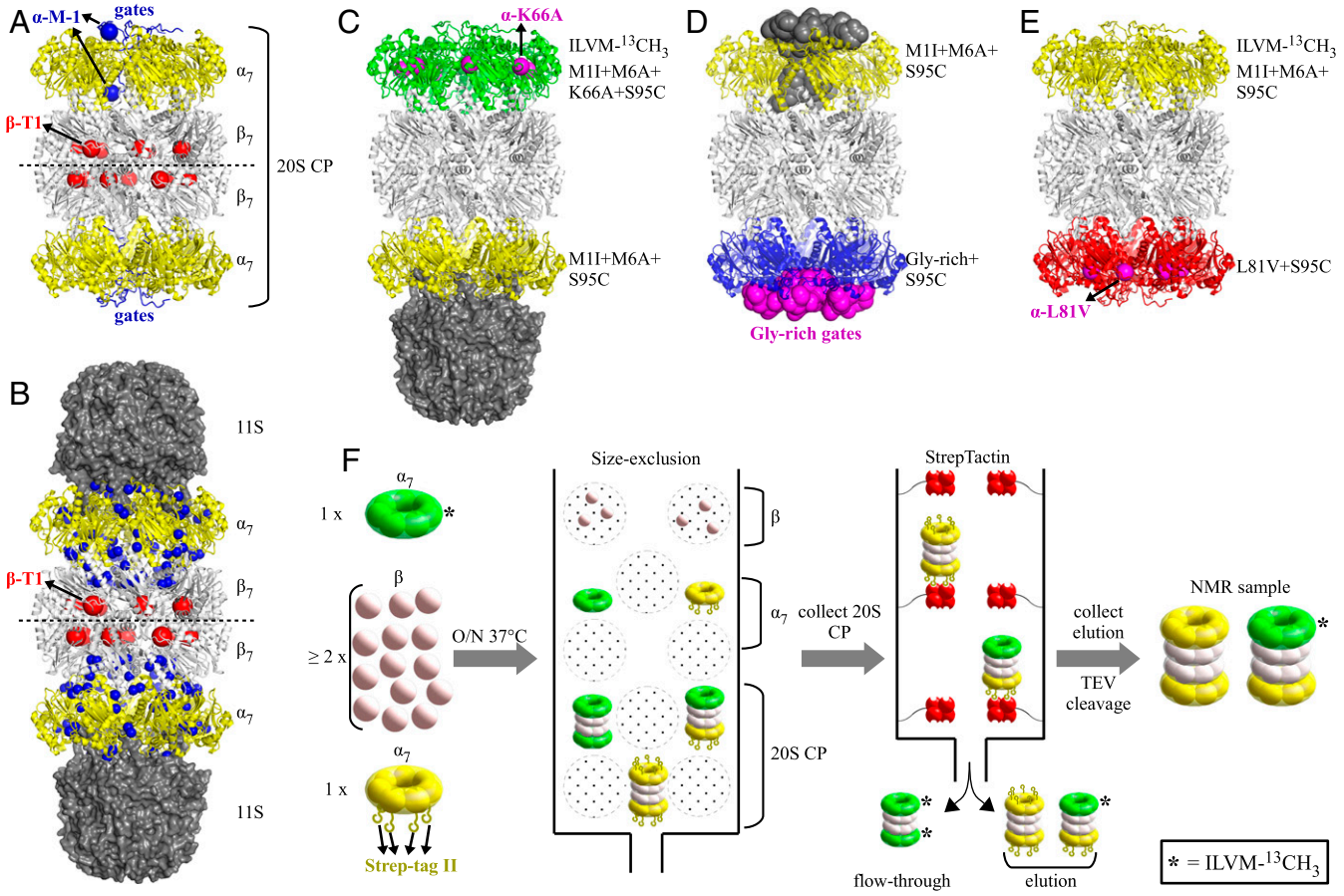

Fig. 1. Design and production of asymmetric 20S CPs to test end-to-end allostery. (*A*) Ribbon diagram structure of the 20S CP, $\alpha_7\beta_7\beta_7\alpha_7$, from *T. acidophilum*, including N-terminal gating residues of α_7-rings indicated in blue [obtained by aligning Protein Data Bank (PDB) entry 2KU1 (19) on the 20S CP from PDB entry 1YA7 (42)]. Five of the seven gates are localized to outside the lumen of the CP, with the terminal residue, M-1, highlighted in one of each of the *out* and *in* gates. The catalytic βT1 residues are depicted with red spheres. (*B*) Three-dimensional structure of the 20S CP (ribbon diagram) in complex with the 11S RP [from *Trypanosoma brucei* (41); space filling model] (42). The blue spheres represent methyl groups reporting on the allosteric pathway connecting activator binding and the catalytic sites (red) (47). (*C*) Designed asymmetric $\alpha_7\beta_7\beta_7\alpha_7$ CP comprising one NMR-active M1I+M6A+K66A+S95C α_7-ring (green) and one NMR-inactive M1I+M6A+S95C (yellow) α_7-ring. Position 66 of each α-subunit on the top ring is highlighted in magenta. The interaction of the K66A α_7-ring with RPs is significantly weakened (51). This construct has been used to test allostery between α_7-rings upon 11S RP binding. (*D*) Asymmetric $\alpha_7\beta_7\beta_7\alpha_7$ CP with M1I+M6A+S95C gates on one α_7-ring, and Gly-rich+S95C gates on a second ring. The gates are depicted in a space-filling representation, with all seven Gly-rich gates assuming the *out* position (21) (magenta), while 5/7 M1I+M6A+S95C gates are *out* (19) (gray). One of the two α_7-rings is ILVM-$^{13}CH_3$ labeled, depending on the experiment. (*E*) Third designed asymmetric $\alpha_7\beta_7\beta_7\alpha_7$ CP, with protomers in one of the α_7-rings (NMR inactive) harboring the L81V mutation (red) that has been shown to affect the allosteric pathway linking activator binding and catalysis (47). Position 81 of each α-subunit on the bottom ring is highlighted in magenta. M1I+M6A+S95C α-subunits (L81) are ILVM-$^{13}CH_3$ labeled. (*F*) Schematic illustrating the generation of asymmetric $\alpha_7\beta_7\beta_7\alpha_7$ CPs. Expression of unlabeled Strep-tag II fusion α molecules (yellow) coupled with Strep-Tactin column purification ensures that the only NMR-active particles are asymmetric, as symmetric ILVM-$^{13}CH_3$–labeled CPs are not tagged and hence are removed in the flow-through. As indicated in the final step, samples containing both NMR-inactive, symmetric 20S CPs and NMR-active, asymmetric CPs are produced, typically in the ratio of 4:6 (a ratio of 1:2 is calculated for the best-case scenario where at least one Strep-tag remains on each yellow α_7-ring during purification [*Materials and Methods*]). For experiments performed with the constructs indicated in *C*–*E*, ratios of 0.46:0.54 (*C*), 0.41:0.59 (*D*), 0.41:0.59 (*E*) were calculated.

subunits of the oligomeric RPs (19S, 11S) forms a salt bridge with the K66 side chain of a CP α-subunit, with other contacts established through hydrogen bonds connecting residues at the terminus of the bound regulator and amino acids 78 to 82 of the α-subunits (25, 26, 30, 32, 35, 42). Although high-resolution structural information is available for complexes involving the different classes of regulator mentioned above (25, 26, 30, 32, 35, 42), a number of biochemical observations have made it clear that 20S CP proteasome function cannot be completely explained on the basis of static structures. For example, the degradation products generated by proteasome 20S CP complexes capped by the 11S RP are affected by mutations to the RP despite the fact that the proteasome active sites, located at the interface of the two β-rings, are far removed from the RPs at the two ends of the structure (45). In addition, atomic force microscopy experiments show gate opening in the yeast proteasome upon binding of inhibitor to active sites (46), while NMR studies of the *T. acidophilum* CP clearly establish a shift in the *in*/*out* gate equilibrium in variants containing prosequences attached to the active-site T1 residues of the β-subunits (β-T1) (47). Finally, the stability of regulator–CP complexes can be influenced by the presence of inhibitors bound to the active sites (48). None of these observations can be explained without invoking an allosteric coupling between the active sites of the β-subunits and gating regions of the α-rings. Structural evidence for this coupling has been obtained through methyl-transverse relaxation optimized spectroscopy (TROSY)-based NMR studies of the *T. acidophilum* CP showing that 1) binding of 11S, 2) mutations of α-L81, a key residue in the proteasome α-subunit that is involved in regulator binding, 3) mutations at the active site β-T1 residue, or 4) binding of an allosteric inhibitor

chloroquine (49), all induced correlated chemical shift changes in a set of methyl groups located along a contiguous structural region (blue spheres in Fig. 1*B*) connecting RP binding sites with catalytic sites that are ~70 Å away (47). Manipulation of the allosteric pathway defined by these chemical shift changes via a series of perturbations including 11S RP binding or mutations at position 81 was shown to modulate proteolysis of α-synuclein, a 20S CP substrate, with different levels of products produced depending on the perturbation (47). Such an allosteric mechanism, in the case of eukaryotic CPs, may play a role in the generation of different antigens for presentation by the MHC class I complex (50).

Having established an allosteric pathway that extends from either end of the 20S CP to the center of the barrel, we now wish to ask whether the network is even more extensive, extending perhaps throughout the complete molecule—between the two α-rings at opposite ends of the complex (~150 Å apart). To this end, we have designed a number of "asymmetric versions" of the 20S CP, with the asymmetry arising from mutations introduced in one of the α-rings of the barrel, as well as from the NMR labeling used, so that perturbations to one ring can be "read out" on the other. In the first case, we exploit the fact that, as described above and in detail previously (19), the N-terminal gates of the α_7 rings are in equilibrium between *in*- (two gates) and *out*- (five gates) conformations, with binding of the 11S RP to the WT α-ring shifting the gate conformation in favor of the *out*-state (19, 43). Thus, by constructing a molecule with a much higher affinity for 11S RP binding at one of the α_7 rings relative to the second and measuring how the *in*/*out* equilibrium is affected in the α_7-ring for which 11S binding is minimal, it is possible to probe whether the allosteric pathway extends between the α_7-rings in the CP. We have also engineered proteasome CPs where the gating termini of an α_7-ring at one end are substituted by Gly-rich sequences that shift the *in*/*out* equilibrium exclusively to the *out* state to explore how this effects gating at the other end of the molecule. In a third test, we make use of L81V mutations that, when introduced into each subunit of the α_7 ring of the CP, lead to chemical shift perturbations (CSPs) from the sites of RP binding (α-rings) to the catalytic threonines of the β-rings (Fig. 1*B*) (47). In contrast to our previous studies where the L81V mutation was introduced into α-protomers from both α_7-rings, we now consider an asymmetric labeling scheme such that 20S CPs are constructed where protomers from only one of the α_7-rings harbor the L81V mutation. If the allosteric network connects both α_7 rings of the proteasome, the CSPs would be expected to extend into the second ring that lacks the mutation. The NMR results from all three diverse CPs are consistent, establishing that the allosteric pathway identified previously (47) does not traverse the length of the full 20S CP proteasome, but rather extends over a single α_7–β_7 element. This study highlights the power of solution NMR spectroscopy, along with asymmetric labeling, for probing allosteric networks in molecular machines that derive from subtle conformational changes that are difficult to characterize using other structural techniques.

Results and Discussion

Generation of Asymmetric 20S CPs. As described above, using a strategy in which asymmetric proteasomes are constructed has allowed us to distinguish between the α-subunits at either ends of the 20S CP barrel. This is achieved in one case by constructing a proteasome CP where each of the α-subunits in one of the α-rings contains the K66A mutation, which has been shown to disrupt the interaction of 20S CPs with RPs (51), while the second α-ring has the WT lysine at position 66. Thus, the 11S regulator can bind to the "K66" α_7 end of the proteasome, with little binding to the K66A side. In order to read out how binding to one α_7 ring affects the *in*/*out* gate equilibrium of the second, the α-K66A ring is rendered NMR active through labeling of the Ile, Leu, Val, and Met methyl groups as $^{13}CH_3$ in an otherwise-perdeuterated background (52, 53), where only one of the prochiral Leu,Val methyls is $^{13}CH_3$ and the other $^{12}CD_3$ (referred to in what follows as ILVM-$^{13}CH_3$ labeling). The second α-ring and both β-rings are NMR silent in our ^{13}C-^{1}H experiments, as they are not isotopically labeled. The use of methyl group probes in NMR studies of high–molecular-weight systems, such as the 670-kDa proteasome or a 850-kDa complex containing a single bound 11S particle, in concert with experiments that exploit a methyl-TROSY effect (54), enables recording of high-quality datasets from which quantitative information can be obtained (55). Fig. 1*C* illustrates the desired asymmetric molecule, where each protomer of the yellow α-ring has the WT K66 amino acid and hence is 11S RP binding competent, while the green, NMR-active, α-ring contains seven K66A mutations that significantly reduce binding (see below). In this manner, it is possible to bind 11S to one ring of the protomer, leading to a shift in the gating equilibrium of that ring, and evaluate whether the shift is also observed at the distal end. Notably, there are three Met residues, M-1, M1, and M6, that are located in each α-gate (Fig. 1*A*), and distinct chemical shifts are observed for the methyl groups of these residues in ^{13}C–^{1}H heteronuclear multiple-quantum correlation (HMQC) spectra for the *in* and *out* states of the gate (19). In the studies described here, we have mutated two of the three methionine gate residues, M1I and M6A, as this improves spectral resolution and, also, quantitation of the *in*/*out* equilibrium (21). Previous NMR studies confirm that these mutations do not affect the gating equilibrium (i.e., ratio of *in*/*out* gates) (21). We have also included an S95C mutation as this substitution reduces the propensity of α_7-rings to form $\alpha_7\alpha_7$ "half-proteasomes," thus improving the isolation of pure 20S CPs, required in our analyses, from smaller complexes.

In a second set of experiments, the molecule shown in Fig. 1*D* has been made, whereby all seven of the gating termini of one of the two α_7-rings are replaced by Gly-rich sequences that we have shown previously significantly decreases the probability of *in* gates (to essentially zero) (21). Thus, by ILVM-$^{13}CH_3$ labeling one of the two rings, it is possible to establish whether an α_7-ring at one end with all gates in the *out* position affects the equilibrium at the other side of the CP barrel, or alternatively, whether some of the Gly-rich gates can be forced to the *in* position by communicating with the second side of the molecule where the gates have the WT *in*/*out* distribution.

As a third and final test of whether allostery extends from one side of the barrel to the other, we have constructed the asymmetric 20S CP illustrated in Fig. 1*E*, where NMR invisible L81V α_7-rings (red; one mutation per protomer) and ILVM-$^{13}CH_3$ labeled α_7-rings with the WT L81 (yellow) are attached on either sides of the CP. In this manner, it is possible to establish whether CSPs introduced by the L81V mutation in each of the protomers of one ring (red) extend to the second α_7-ring (yellow), which would provide strong evidence of a continuous allosteric pathway spanning the length of the proteasome.

Fig. 1*F* illustrates the protocol that has been developed for the preparation of asymmetric 20S CPs of the type shown in Fig. 1 *C*–*E*. In this approach, ILVM-$^{13}CH_3$ α_7-rings (green) and natural abundance α_7-rings with an N-terminal Strep-tag II (56) (yellow) were mixed in a 1:1 ratio in the presence of an excess of natural abundance β-subunits and incubated overnight at 37 °C. Size-exclusion chromatography was used to isolate the fully assembled $\alpha_7\beta_7\beta_7\alpha_7$ CPs from lower mass molecules, such as α_7-rings. The CPs were subsequently passed through a Strep-Tactin column; the symmetric particles with ILVM-$^{13}CH_3$ α_7-rings on both sides of the barrel are removed in the flow-through, as these are not able to bind to the Strep-Tactin resin. The eluted fraction that is used to make the NMR sample, contains not only the desired asymmetric 20S CP with just one ILVM-$^{13}CH_3$ labeled α_7-ring (green–yellow complexes) but also a symmetric CP with Step-tagged natural abundance α_7-rings on both sides (yellow–yellow complexes). These symmetric CPs are not ^{13}C labeled,

however, and therefore they are effectively NMR silent. In what follows, α_7-rings that are ILVM-$^{13}CH_3$ labeled will be indicated with an asterisk (*) in all figures, with the various types of rings used in NMR experiments distinguished by different colors. Assuming that the Strep-tags remain intact, 66.7% of all of the particles present in the final NMR sample are predicted to have the desired asymmetric labeling. However, in practice, this percentage is smaller due to the partial degradation of the Strep-tag by the 20S CP itself during the assembly reaction and purification. Further details concerning sample production are presented in *Materials and Methods*, along with a formula for calculating the percentage of desired asymmetric particles in the NMR sample based on the fraction of CPs in the Strep-Tactin column flow-through. Comparison of ^{13}C–^{1}H HMQC spectra of an asymmetric 20S CP sample, prepared as described above, with spectra of symmetric 20S CPs and of intentionally uniformly scrambled particles where labeled and natural abundance α-protomers are randomly distributed in both α_7-rings of the CP indicates that no significant scrambling between protomers of the α_7-rings occurs during the production of samples or NMR data acquisition (*SI Appendix*, Fig. S1).

Binding of 11S to Isolated α_7-Rings. Prior to recording experiments with the asymmetric 20S CP samples, we measured the interaction between 11S RPs and single α_7-rings to establish the extent to which the K66A mutation reduces their binding affinity. As expected, ^{13}C–^{1}H HMQC spectra of ILVM-$^{13}CH_3$ M1I+M6A+S95C α_7 and ILVM-$^{13}CH_3$ M1I+M6A+K66A+S95C α_7, recorded at 40 °C and 600 MHz, are very similar in the absence of 11S (black contours in Fig. 2 *A* and *D* and *SI Appendix*, Fig. S2), providing strong evidence that the K66A mutation does not change the overall structure of the α_7-ring. Integration of cross-peaks derived from M-1 that report on the *in*/*out* gate equilibrium establish that, for both α_7 variants, two gates of the seven are in the *in* conformation (Table 1), so that the *in*/*out* ratio is close to 0.4. The observed populations of *in* and *out* gates are in agreement with those previously measured for the WT α_7 (19), indicating that the introduced mutations do not affect the gating thermodynamics. Finally, similar timescales of exchange between *in* and *out* gate conformations are measured for the K66 and K66A constructs (*SI Appendix*, Fig. S3) via magnetization exchange experiments (19), although it is worth emphasizing that it is the thermodynamics, rather than the kinetics of gating, that are of interest here.

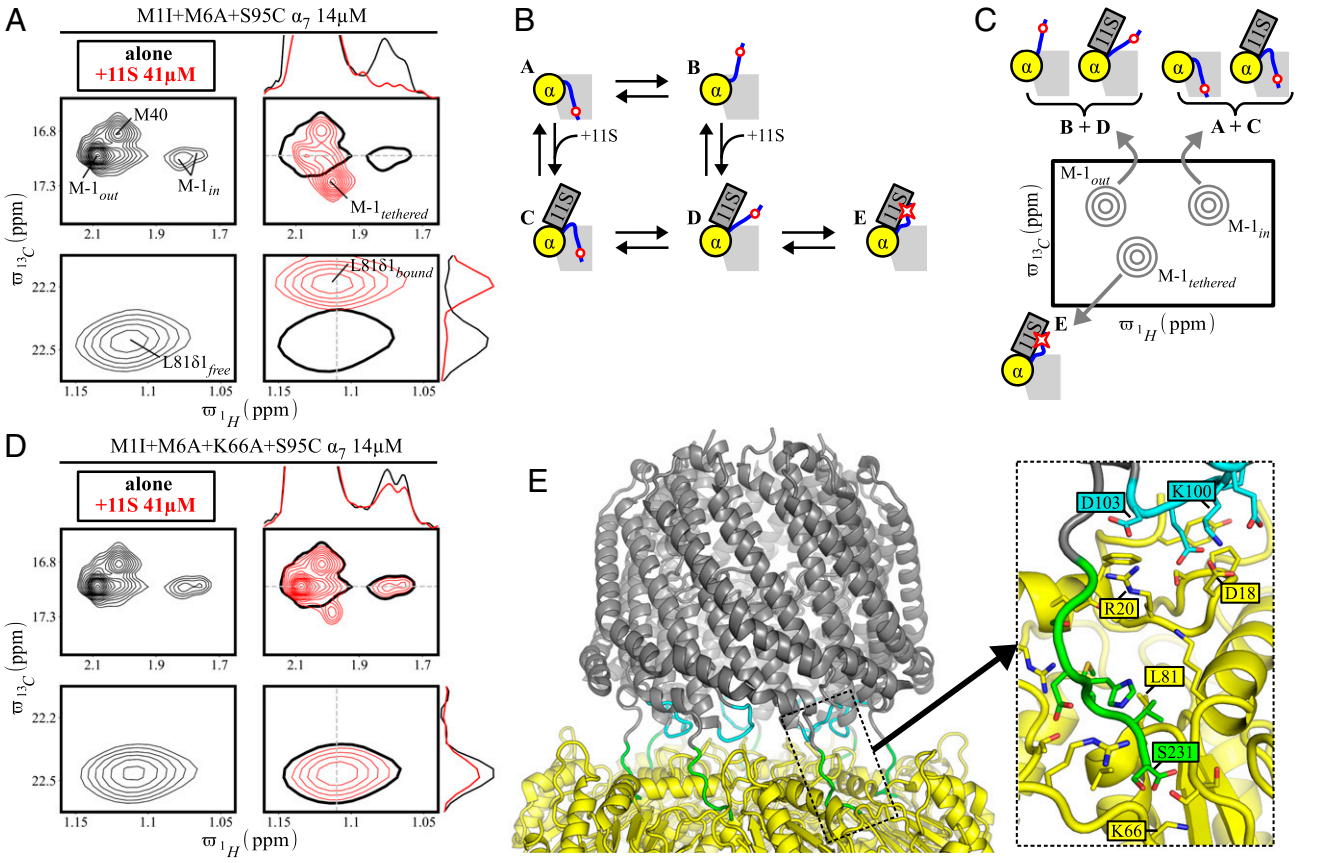

Fig. 2. Binding of 11S RPs to α_7-rings. (*A*) Binding of 11S to M1I+M6A+S95C α_7 is established by the appearance of a new cross-peak derived from M-1, M-$1_{tethered}$. Note the decrease in intensities of peaks from *in* gate states upon 11S binding. Also shown are spectral regions highlighting L81δ1, a residue reporting on an 11S binding interaction only present for the K66 α_7-ring. Spectra in black(red) are measured on α_7 (+11S RP) samples. Single black contours in spectra of α_7+11S RP (red) are derived from α_7 in the absence of the RP. One-dimensional traces at ϖ_{13_C} = 17 ppm for M-1, and for L81 at ϖ_{1_H} = 1.11 ppm are shown. (*B*) Five-state model depicting *in* (**A**+**C**), *out* (**B**+**D**), and *tethered* (**E**) gating conformations that provides the simplest explanation of the observed NMR spectrum. The light gray area indicates the lumen of the proteasome, and α-M-1 is denoted by a red sphere (*in* and *out* states) or a red star (*tethered* state). (*C*) Schematic ^{13}C–^{1}H correlation map showing the positions of the M-1 cross-peaks and the states, **A**–**E**, from which they are derived. (*D*) As in *A* but with M1I+M6A+K66A+S95C α_7-rings. (*E*) Portion of the 3D structure of the 20S CP–11S RP complex (42), focusing on the interface between the α_7-ring (yellow) and the 11S RP (gray); the two interaction sites on the 11S RP are colored in green and cyan (42). The magnified plot on the *Right* shows the main site of interaction (green) stabilized by a salt bridge between the C-terminal carboxylate group of the 11S RP (S231) and α-K66, as well as by hydrogen bonds between 11S RP C-terminal residues and amino acids on the α-subunits, such as L81. The second site (cyan) involves contacts between residues E98–D103 of the 11S RP, and Y8 and S16–F22 of the α-subunits.

Table 1. Populations of *in*/*out*/*tethered* gates for K66 or K66A single α_7-ring particles, either unbound or 11S RP bound

		Leu81	Met-1			
α_7 Construct	α_7:11S	*Bound**	*In*	*Out*	*In/out*	*Tethered*
M1I+M6A+S95C α_7	1:0	0%	27.3 ± 1.1%	72.7 ± 2.8%	0.38 ± 0.02	0%
	1:3	89 ± 3%	12.0 ± 0.8%	24.4 ± 4.0%	0.49 ± 0.09	63.6 ± 4.5%
M1I+M6A+K66A+S95C α_7	1:0	0%	27.3 ± 1.0%	72.7 ± 3.2%	0.38 ± 0.02	0%
	1:3	3 ± 2%	23.2 ± 1.7%	57.7 ± 2.4%	0.40 ± 0.03	19.2 ± 1.1%

Observed populations were calculated from peak volumes and converted to populations of the five states highlighted in Fig. 2*B*, as described in the text. Peak volumes were corrected for differential transverse relaxation in the case of M-1 (see *Materials and Methods* for details).

*Percent 11S RP bound, as reported by ratio of volumes of "bound" and "free" L81δ1 peaks (Fig. 2 *A* and *B*). The chemical shift of L81δ1 responds to an interaction involving the C-terminal tail of the 11S RP and α-subunit residues 78 to 82. In the case of WT α_7-rings, these contacts are present, and hence L81δ1 is a good probe of binding. In the case of the K66A mutant, the binding interaction reported by L81 is no longer present (no CSP; see text). Binding can still occur, however, through a second interaction discussed in the text, and the fraction bound determined as described in the text and *Materials and Methods*.

It should be noted that in any analysis of peak integrals in terms of populations care must be taken to ensure that relaxation effects do not bias the results. Throughout this work, we have measured transverse relaxation rates and corrected peak intensities, as described in *Materials and Methods* and in previous publications (21, 57). Addition of perdeuterated 11S to ILVM-$^{13}CH_3$ M1I+M6A+S95C α_7 leads to several changes in the NMR spectrum (red contours in Fig. 2*A*), including the appearance of a new peak for L81δ1 that derives from the *bound* state, as previously described by Sprangers and Kay (58). This new peak results from the interaction between the C-terminal residues of the 11S RP and amino acids 78 to 82 of the α-subunits that form a binding pocket (see below) (42). In addition to the CSP for L81δ1, several changes are also noted in the methionine region of the spectrum. A new peak is observed for M-1, a residue that is distal from the 11S RP binding pocket, derived from what we refer to as a *tethered* state involving the gate. NMR spin relaxation experiments provide evidence that this new peak reflects a direct interaction between the gate and the 11S RP, as methyl ^{1}H transverse relaxation rates for M-1 (*Materials and Methods*) increase from 6.8 ± 0.1 s^{-1} (*out* state) to 31.5 ± 0.5 s^{-1} (*tethered* state), which is consistent with a restriction of the motions of the N-terminal gating residues of the α-subunit in the tethered conformation. Binding of 11S leads to a reduction in both *in* and *out* peaks, although the *in*/*out* ratio is still very close to 0.4 (Table 1). Interestingly, the total fraction of *bound* protein, as measured by the amplitude of the bound/free peaks for L81δ1, ∼90%, is significantly larger than the fraction of *tethered* M-1, ∼64%. Fig. 2*B* presents a model that is consistent with these data where, for simplicity, the focus is on a single gate (colored blue) of the seven in the α-ring. In Fig. 2*B*, the gate residue M-1 is highlighted by a red circle in the untethered state while the *tethered* M-1 is delineated with a star and shown schematically as binding to the 11S RP. There are two states for the 11S unbound form, **A** and **B**, corresponding to gate *in* and *out*, respectively, and three bound conformers denoted as **C** (M-1 *in*, 11S *bound*), **D** (M-1 *out*, 11S *bound*), and **E** (M-1 *tethered*, 11S *bound*). In what follows, we distinguish between an *out* and a *tethered* gate in the bound form, although *tethered* gates are also localized to outside of the proteasome lumen, by whether M-1 contacts the 11S RP (state **E**) or is free (state **D**). The fact that L81 reports a larger fraction bound than M-1 reports a fraction *tethered* indicates that the $\mathbf{C} \leftrightarrow \mathbf{D} \leftrightarrow \mathbf{E}$ equilibrium is not completely skewed toward the **E** state. Quantitation of the relative populations of the five states **A**–**E** can be achieved by noting that each of the M-1 cross-peaks in Fig. 2*A* can be assigned to specific states, as indicated in Fig. 2*C*. Thus, $p(in)$, the fractional population of gates in the *in* state can be expressed in terms of the fractional populations of states **A** and **C**, as $p(in) = p(\mathbf{A}) + p(\mathbf{C})$, with $p(out)$ and $p(tethered)$ [denoted as $p(tet)$, in what follows], given by $p(out) = p(\mathbf{B}) + p(\mathbf{D})$, and $p(tet) = p(\mathbf{E})$, respectively. By measuring volumes of each of the M-1 peaks, $p(in)$, $p(out)$, and $p(tet)$ values are obtained (Fig. 2*C*), and from the relative volumes of the L81δ1 cross-peaks reporting on 11S bound and unbound rings, the fraction of bound α_7 particles is generated, corresponding to $p(\mathbf{C}) + p(\mathbf{D}) + p(\mathbf{E})$. A set of five linear equations is thus obtained that can be solved (*Materials and Methods*) to give the populations of the five states: $\mathbf{A} = 3.1 \pm 1.8\%$, $\mathbf{B} = 7.9 \pm 4.5\%$, $\mathbf{C} = 8.9 \pm 1.9\%$, $\mathbf{D} = 16.5 \pm 4.1\%$, and $\mathbf{E} = 63.6 \pm 4.5\%$. We refer to this high-affinity bound conformation as state I (11S RP + K66 α_7 ring), and to the binding site as site I, to distinguish it from the much lower affinity bound state II associated with the interaction between the 11S RP and the K66A mutated α_7-ring (see below). In addition to the probabilities, $p(\mathbf{J})$ $\mathbf{J}\in\{\mathbf{A}–\mathbf{E}\}$, defined above, it will be convenient in what follows to define conditional probabilities such as $p(in|\mathrm{I^{BD}}) = p(\mathbf{C})/[p(\mathbf{C}) + p(\mathbf{D}) + P(\mathbf{E})]$, $p(out|\mathrm{I^{BD}}) = p(\mathbf{D})/[p(\mathbf{C}) + p(\mathbf{D}) + p(\mathbf{E})]$ and $p(tet|\mathrm{I^{BD}}) = p(\mathbf{E})/[p(\mathbf{C}) + p(\mathbf{D}) + p(\mathbf{E})]$, corresponding to the probabilities of *in*, *out*, and *tethered* gates for the I bound conformation ($\mathrm{I^{BD}}$). Thus, for example, $p(\mathbf{C}) = p(\mathrm{I^{BD}})\cdot p(in|\mathrm{I^{BD}})$, where $p(\mathrm{I^{BD}})$ is the fraction of α_7-rings bound to 11S. Within the bound conformation I, comprising states **C**, **D**, **E**, $p(in|\mathrm{I^{BD}}) = 10.0 \pm 2.0\%$, $p(out|\mathrm{I^{BD}}) = 18.5 \pm 4.1\%$, and $p(tet|\mathrm{I^{BD}}) = 71.5 \pm 5.4\%$. Note that as the equilibria between **C**, **D**, and **E** are all first-order, $p(in|\mathrm{I^{BD}})$, $p(out|\mathrm{I^{BD}})$, and $p(tet|\mathrm{I^{BD}})$ are independent of the 11S concentration. The dissociation constant for binding of 11S to M1I+M6A+S95C α_7, $K_D^{\mathrm{I}} = ([\mathbf{A}] + [\mathbf{B}]) \cdot [\mathbf{L}]/([\mathbf{C}] + [\mathbf{D}] + [\mathbf{E}])$, where **[L]** is the concentration of free 11S, is calculated to be 3.5 ± 1.2 μM, based on the fractional populations of the states listed above and the total 11S and α_7 concentrations used (*Materials and Methods*).

Introduction of the αK66A mutation in each subunit reduces binding of the α_7-ring to the 11S RP (red contours in Fig. 2*D*), with no changes in the Ile and Leu/Val regions of the ^{13}C–^1H correlation map (*SI Appendix*, Fig. S2), and no detectable *bound* peak for L81. The absence of a chemical shift change for L81 is expected, as the interaction between the C-terminal residues of the 11S RP and each of the α-subunit binding pockets is severely impaired by the K66A mutation. Notably, however, a small peak corresponding to the *tethered* state is observed for M-1, indicating that a second, weak interaction with the 11S RP is present. Insight into why an interaction still persists can be obtained from the high-resolution X-ray structure of the *T. acidophilum* CP:11S RP complex showing that there are two sites of contact between the WT α_7-ring and 11S RPs, with the first involving a salt bridge between the 11S C-terminal residue S231 and K66 of

the α-ring that is responsible for the shift in the resonance position of the proximal L81 peak (Fig. 2*A*) and the second site including interactions between E98–D103 of the activation loop of 11S and residues Y8 and S16–F22 of the α_7-ring (Fig. 2*E*) (42). In the case of binding of 11S to WT α_7, both sets of interactions are formed, but in the context of the K66A mutation only the second interaction set is preserved and the binding is, therefore, weaker. As with the K66 α_7-ring–11S interaction, discussed above, it is possible to derive a set of linear equations that relate populations of the five states of Fig. 2*B* to intensities of the M-1 cross-peaks. However, in this case, the system is underdetermined, as the fractional population of 11S bound rings, $p(\mathbf{C}) + p(\mathbf{D}) + p(\mathbf{E})$, cannot be obtained from the L81 resonance that is no longer sensitive to binding in the mutant. We therefore assume that the relative populations of *tethered* states are the same when the 11S is bound in conformations I or II, that is $p(tet|\mathrm{II}^{\mathrm{BD}}) = p(\mathrm{tet}|\mathrm{I}^{\mathrm{BD}}) = 71.5\%$, from which it follows that $\mathbf{A} = 20.9 \pm 0.8\%$, $\mathbf{B} = 52.2 \pm 2.0\%$, $\mathbf{C} = 2.3 \pm 1.7\%$, $\mathbf{D} = 5.4 \pm 2.0\%$, and $\mathbf{E} = 19.2 \pm 1.2\%$, and that $p(in|\mathrm{II}^{\mathrm{BD}}) = 8.6 \pm 5.8\%$ and $p(out|\mathrm{II}^{\mathrm{BD}}) = 20.0 \pm 7.0\%$. It is noteworthy that $p(in|\mathrm{II}^{\mathrm{BD}})$ and $p(out|\mathrm{II}^{\mathrm{BD}})$ are the same as $p(in|\mathrm{I}^{\mathrm{BD}})$ and $p(out|\mathrm{I}^{\mathrm{BD}})$, respectively, to within experimental error, indicating that the gating distribution in either K66- or K66A-bound rings is very similar. Finally, the dissociation constant for M1I+M6A+K66A+S95C α_7 and 11S, $K_{\mathrm{D}}^{\mathrm{II}} = ([\mathbf{A}] + [\mathbf{B}]) \cdot [\mathbf{L}]/([\mathbf{C}] + [\mathbf{D}] + [\mathbf{E}])$, can be calculated from the $p(\mathbf{J})$ values and the total 11S and α_7 protein concentrations used (*Materials and Methods*). A value of $K_{\mathrm{D}}^{\mathrm{II}} = 101 \pm 14$ μM is obtained, 30 times larger than $K_{\mathrm{D}}^{\mathrm{I}}$. The overall *in*/*out* ratio for M1I+M6A+K66A+S95C α_7 in the presence of 11S is still close to 0.4 (0.40 ± 0.03; Table 1).

Testing Models of Allostery through Binding of 11S to the 20S Core Particle. Our results are consistent with two sites of interaction between a WT α-ring and an 11S RP, as expected from the X-ray structure of the 20S CP:11S RP complex (42) and, furthermore, highlight that the α−K66A mutation eliminates the high-affinity contact involving the C-terminal carboxylic group of 11S. With the values of $K_{\mathrm{D}}^{\mathrm{I}}$ and $K_{\mathrm{D}}^{\mathrm{II}}$ available, it is now possible to test whether binding of 11S to predominately one side of the 20S CP leads to changes in the gating equilibrium at the other end. As described above, not all of the 20S particles produced using the protocol in Fig. 1*F* are the desired asymmetric molecules, with one K66A (ILVM-$^{13}CH_3$) and one K66 (unlabeled) α_7-ring at each end (Fig. 3*A*). Rather, a mixture is obtained comprising NMR-invisible symmetric 20S CPs (K66 α_7-rings at both ends) and the desired asymmetric CPs. Based on the quantity of protein present in the flow-through and the elution fractions from the Strep-Tactin column, the percentage of the asymmetric 20S CPs is estimated to be 54% (*Materials and Methods*), rather than the maximum 66.7% that is predicted assuming that not all of the Strep-tags are cleaved from each of the α_7 rings (i.e., only one tag is required per ring to bind the column). Note that a mixture of different CPs does not affect the accuracy of the analysis, so long as spectral signal-to-noise is not limiting, because the only NMR signal observed is derived from the asymmetric particles that report on the allostery. Binding of the 11S RP to the symmetric, NMR-invisible particles must be taken into account, however, to calculate the fractional population of the 11S-bound asymmetric particles, as described in *Materials and Methods*.

Fig. 3 *B*, *Left*, shows the region of a ^{13}C–^{1}H HMQC spectrum of the 20S CP in the absence of the 11S RP (40 °C and 800 MHz) that contains correlations from M-1. The relative intensities of the M-1_{out} and M-1_{in} cross-peaks in the apo case, 0.39 ± 0.01, indicates that the *in*/*out* gate ratio is close to the expected value of 0.4 (Table 2), corresponding to the situation where two gates are *in* and five are *out* of the proteasome lumen, which further establishes that the gating thermodynamics are not affected by the K66A mutation. Upon addition of a threefold molar excess of the 11S RP over the 20S CP (Fig. 3 *B*, *Right*), a small decrease in the intensities of the M-1_{in} correlations is observed, along with the appearance of a peak derived from tethering of M-1 to the 11S particle. Table 2 lists the relative fractions of *in*, *out*, and *tethered* gates in this case. These fractions are with reference to the gates of the K66A α_7-ring, as only these are NMR active. Since $K_{\mathrm{D}}^{\mathrm{I}}$ (3.5 ± 1.2 μM) and $K_{\mathrm{D}}^{\mathrm{II}}$ (101 ± 14 μM) are known, the fraction of CPs bound with 11S at the high-affinity [K66 ring; $p(\mathrm{I}^{\mathrm{BD}})$] and low-affinity [K66A ring; $p(\mathrm{II}^{\mathrm{BD}})$] sites, referred to as sites I and II, respectively (see above), can be calculated using a competitive binding model (59) that takes into account the relative concentrations of symmetric and asymmetric proteasome particles in solution and the total concentration of added 11S (*Materials and Methods*). Under the assumption that the gates at opposite ends of the proteasome operate independently so that binding of RP to one end of the barrel has no effect on the gate distribution at the opposite end (i.e., no cooperativity), the observed gating equilibrium at the NMR-active M1I+M6A+K66A+S95C α_7-rings will not be affected by the positions of the gates in the (NMR-silent) M1I+M6A+S95C α_7-rings. The predicted populations of *tethered*, *in*, and *out* gates for the K66A ring of the 20S CP complex in this case are thus given by the following:

$$\begin{aligned} p(tet) &= p\left(\mathrm{II}^{\mathrm{BD}}\right) \cdot p\left(tet|\mathrm{II}^{\mathrm{BD}}\right) \\ p(in) &= p^{o}(in) \cdot \left(1 - p\left(\mathrm{II}^{\mathrm{BD}}\right)\right) + p\left(in|\mathrm{II}^{\mathrm{BD}}\right) \cdot p\left(\mathrm{II}^{\mathrm{BD}}\right) \\ p(out) &= \left(1 - p^{0}(in)\right) \cdot \left(1 - p\left(\mathrm{II}^{\mathrm{BD}}\right)\right) + p\left(out|\mathrm{II}^{\mathrm{BD}}\right) \cdot p\left(\mathrm{II}^{\mathrm{BD}}\right), \end{aligned} \quad [1]$$

where $p^0(in) = 2/7$ (19) is the *in* gate population in the absence of 11S. Values of $p(x|\mathrm{II}^{\mathrm{BD}})$ with $x = \{tet, in, out\}$ are given in the previous section and $p(\mathrm{II}^{\mathrm{BD}}) = 0.24 \pm 0.03$ (*Materials and Methods*). Calculated $p(tet)$, $p(in)$, and $p(out)$ obtained from Eq. **1** (absence of allostery) are listed in Table 2. Notably, these values are in excellent agreement with experimental observations.

As a second limiting model, we consider the case where gates at opposite ends of the proteasome are maximally coupled. Thus, binding of the 11S RP to one end of the barrel, and the concomitant shift in the *in*/*out* equilibrium toward the *out* state in the 11S bound conformation, will propagate to the second unbound end and affect the gating equilibrium at this location as well. In this scenario, substrate entry would be facilitated at the unbound end, at least for intrinsically disordered proteins or proteins with substantial regions of disorder that do not require active unfolding to enter into the proteasome barrel for degradation (49). Because $K_{\mathrm{D}}^{\mathrm{I}} << K_{\mathrm{D}}^{\mathrm{II}}$, the added 11S RP will bind much more extensively to site I [$p(\mathrm{I}^{\mathrm{BD}}) = 0.90$] than to site II [$p(\mathrm{II}^{\mathrm{BD}}) = 0.24$], increasing the population of K66 gates (site I) in the *out* and *out*+*tethered* conformations [$p(out|\mathrm{I}^{\mathrm{BD}}) + p(tet|I^{BD}) = 0.90 \pm 0.07$] from the canonical $p(out)$ value of 5/7 in the absence of 11S. As the gate distribution in the unbound K66A α_7-ring is slaved to the distribution in the 11S RP-bound K66 ring in this second model (*SI Appendix*), the net effect is a shift in the K66A gate populations, as well. Values of $p(in)$, $p(out)$, and $p(tet)$ can be calculated (for the NMR observable K66A α_7-site of the 20S CP, site II) by considering all of the different 11S bound/unbound configurations, as illustrated in Fig. 3*C*, along with expressions that are listed there and described in more detail in *SI Appendix*. Table 2 lists the calculated *P* values. These deviate considerably from what is observed experimentally. Notably $p(in)$ calculated for the case of maximum allostery is significantly smaller than the observed value, leading to a much reduced $p(in)/p(out)$ ratio than what is measured (0.15 ± 0.03 vs. 0.42 ± 0.02). It is clear that this model does not describe the data, while the assumption of no cooperativity between sites, and hence no communication between

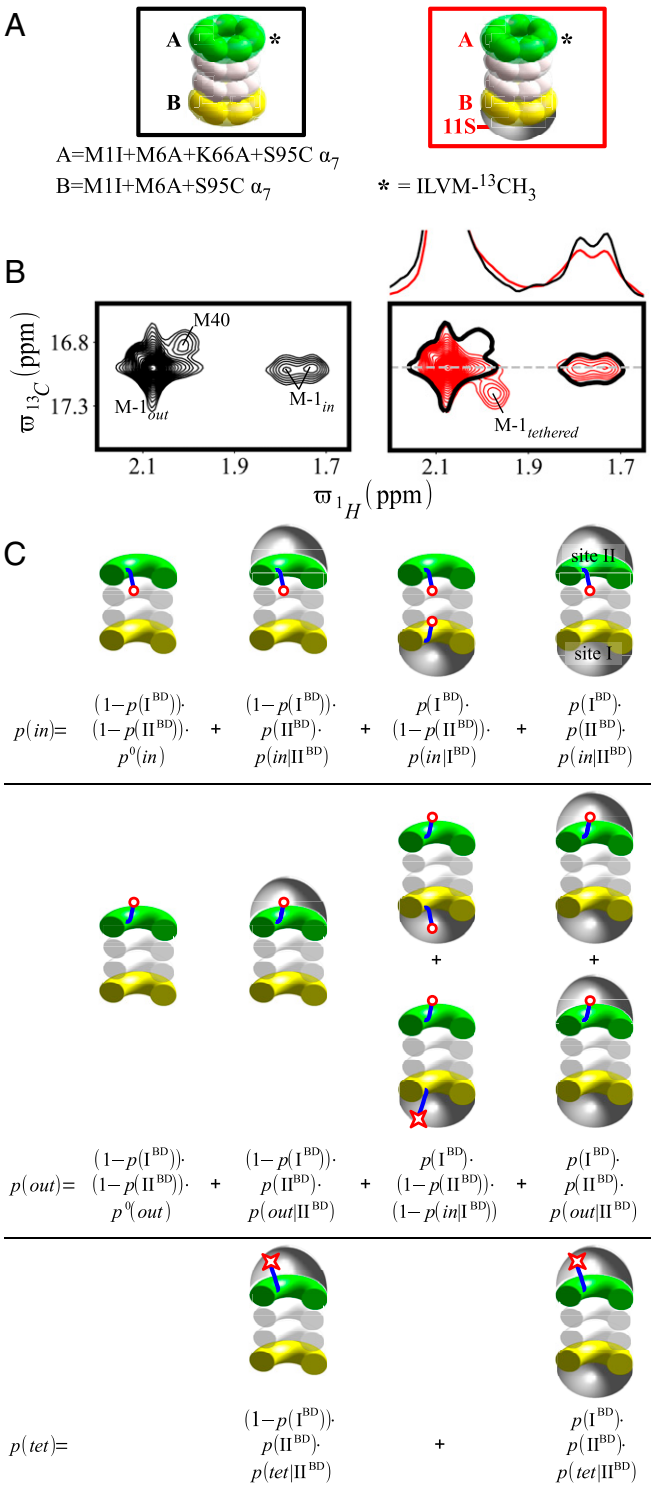

Fig. 3. Testing long-range allostery in the 20S CP upon binding 11S RPs. (*A*) A sample was prepared (Fig. 1) containing a mixture of symmetric CPs (where both α_7-rings of the complex are M1I+M6A+S95C and are not NMR labeled) and asymmetric CPs (one α_7-ring, M1I+M6A+K66A+S95C, is ILVM-$^{13}CH_3$ labeled and a second ring, M1I+M6A+S95C, is unlabeled). Only the asymmetric CP, shown, gives rise to NMR signals. ILVM-$^{13}CH_3$–labeled α_7-rings are indicated with an asterisk (*). (*B*) Spectra highlighting α–M-1 correlations in the absence (black) and presence (red) of threefold molar excess of 11S RP over the 20S CP. One-dimensional slices are shown at ϖ_{13c} = 17 ppm. (*C*) Shown are the four possible bound/unbound 20S configurations (20S:11S = 1:0, 1:1 with 11S binding on top—site II, 1:1 with 11S binding on bottom—site I, and 1:2). The population of *in* (*Top*), *out* (*Middle*), and *tet* (*Bottom*) gating conformations

the α_7-rings at the opposite ends of the barrel, leads to calculated *P* values that are in good agreement with observations.

Testing Models of Allostery through Gate Mutation. As a second probe of long-range allostery in the 20S CP system, we have generated an additional set of complexes in which one of the α_7-rings is of the M1I+M6A+S95C variety with a second ring consisting of protomers in which the gates are enriched in Gly residues (Gly-rich gate, MGGSEGGGSEGGGA, vs. M1I+M6A sequence, MGIQQGQAAYDRAI). We have previously shown that Gly-rich gates have a very low propensity to assume the *in* position, with the intrinsic probability of an individual gate entering the lumen of the proteasome decreasing from ~96% for the M1I+M6A gate, corresponding to $p(in) = 28.4\%$ (21), to less than 2% for a Gly-rich gate [$p(in) < 2\%$]. Our choice of the Gly-rich α_7-ring maximizes the chance of observing long-range allostery that connects both ends of the 20S CP, as the gating propensities at the two ends of the asymmetrically constructed molecule are drastically different. Quantification of the intensities of the M-1_{out} and M-1_{in} peaks for symmetric 20S CP samples composed of either both M1I+M6A+S95C α_7-rings or both Gly-rich α_7-rings gives the expected $p(in)$ values of about 28% and 0%, respectively (Fig. 4 *A* and *B* and Table 3). Small differences are observed in spectra generated from the corresponding asymmetric 20S CP samples (Fig. 4 *C* and *D* and Table 3), where each of the α_7-rings was ILVM-labeled individually. In particular, an increased $p(in)$ value of ~35% is quantified from particles where the M1I+M6A+S95C α_7-ring is NMR active (Fig. 4*C* and Table 3). This increase is opposite to what would be expected in the case of positive allostery, suggesting, perhaps, negative cooperativity between ends of the molecule. However, an alternative explanation is one where an intermolecular association between CPs occurs, such that a gate from an (NMR-active) M1I+M6A+S95C α_7-ring on one CP penetrates the lumen of an adjacent proteasome at an end with a Gly-rich α_7 ring. As the Gly-rich gates are all in the *out* position, they do not obstruct the entrance into the proteasome lumen. In the NMR sample used for the experiments of Fig. 4*C*, the molar fractions of asymmetric and symmetric Gly-rich 20S CPs are in the ratio 59%:41%, so that 70% of the α_7 rings attached to CPs are of the Gly-rich variety. Therefore, to test this hypothesis, we acquired an HMQC spectrum of a mixture of ILVM-$^{13}CH_3$

for the K66A α_7-ring, site II, is given for each of the configurations shown, described in detail in *SI Appendix*. Similarly, *in*, *out*, and *tet* gating states are possible for the K66 ring as well (site I). However, configurations of site I gates are illustrated only for the cases where gates in site II (that are observed in NMR experiments) are slaved to them, and this occurs only in the case where the 11S RP is bound to site I, but not to site II. As described in detail in *SI Appendix*, our model is based on the assumption that binding of the 11S RP at one site of the CP leads to the same gating equilibria at that site as for an isolated α_7-ring that is 11S RP bound. Thus, when the 11S RP is bound to site II, irrespective of whether site I is in the bound state or not, $p(in|II^{BD})$, $p(out|II^{BD})$, and $p(tet|II^{BD})$ values are given by the corresponding *P* values measured for the isolated M1I+M6A+K66A+S95C α_7-ring; for these cases, therefore, the gate configuration in site I is irrelevant. The $\alpha_7\beta_7\beta_7\alpha_7$ 20S CP is represented by four stacked tori, where the ILVM-$^{13}CH_3$–labeled K66A α_7-ring is in green, the unlabeled K66 α_7-ring is in yellow, and the two β_7 rings are in white. The α gates are highlighted in blue, and α-M-1 is indicated by a red sphere (*in* and *out* states) or a red star (*tethered* state). The 11S CP is represented by a gray spherical shell. The analytical expressions for the populations of *in*, *out*, and *tethered* states are as indicated. In the listed equations, $p(I^{BD})$ and $p(II^{BD})$, are the fractional populations of high-affinity (K66 rings; site I) and low-affinity (K66A rings; site II) sites that are bound to the 11S RP, $p^0(in) = 2/7$ and $p^0(out) = 5/7$ are the fraction of *in*/*out* states when 11S is not bound (19, 21, 47), and $p(x|II^{BD})$ x={*in*, *out*, *tet*} is the fraction of gates in an 11S-bound K66A α_7-ring (11S binding site II) that are either *in*, *out*, or *tet*, as determined in this work; $p(x|I^{BD})$ is defined the same way as $p(x|II^{BD})$, with the exception of an 11S-bound K66 α_7-ring.

Table 2. Experimental and predicted populations of *in*/*out*/*tethered* gates in the 20S CP with and without the 11S RP

20S CP:11S RP*		*In*	*Out*	*In/out*	*Tethered*
1:0	Observed	28.1 ± 0.8%	71.9 ± 1.3%	0.390 ± 0.013	0%
	Expected	28.6%	71.4%	0.4	0%
1:3	Observed	25.8 ± 0.5%	61.3 ± 1.8%	0.42 ± 0.02	12.9 ± 0.8%
	Expected without allostery	23.8 ± 1.4%	59.0 ± 2.0%	0.40 ± 0.02	17.2 ± 2.4%
	Expected with maximum allostery	11.0 ± 1.8%	71.8 ± 2.8%	0.15 ± 0.03	17.2 ± 2.4%

Observed populations are calculated from peak volumes, corrected for differential transverse relaxation. See *Materials and Methods* for details about concentrations used.

*Concentrations of 20S CP and 11S RP are 22 and 65 μM, respectively. Note that there are two populations of 20S CPs, corresponding to the NMR invisible symmetric complex where both α_7-rings are MII+M6A+S95C (46%), and a second 20S CP (54%) comprising one M1I+M6A+K66A+S95C α_7-ring (NMR active) + one NMR inactive M1I+M6A+S95C α_7-ring.

M1I+M6A+S95C symmetric 20S CPs and unlabeled Gly-rich symmetric proteasomes in the ratio 3:7, the same ratio of each type of ring as in the asymmetric 20S CP sample (Fig. 4*E*). In addition, the same net concentration of CPs was used as for the asymmetric 20S CP sample (26 μM). An increase in $p(in)$ to about 35% is observed in this mixture (Fig. 4*E*), exactly as detected for asymmetric 20S CP particles where the M1I+M6A+S95C α_7-ring is NMR active (Fig. 4*C*). This indicates that, instead of long-range allostery, the slight elevation in $p(in)$ is fully explained by an intermolecular association. Consistent with this result, we do not observe CSPs that would normally accompany triggering of an allosteric pathway in either half of the asymmetric molecule (*SI Appendix*, Fig. S4), indicating that the gating status at one end of the particle is not transmitted to the other half of the CP.

The appearance of an additional peak in asymmetric samples where the Gly-rich α_7-ring is ILVM labeled (compare Fig. 4 *B* and *D*) is of interest. Both its position and measured relaxation properties indicate that it is derived from the *out* state. For example, ^{1}H transverse relaxation rates quantified from the pair of peaks in Fig. 4*E* at 2.08 and 1.98 ppm are small, 12 and 16 s^{-1}, respectively, in contrast with values higher than 40 s^{-1} measured for the *in* peaks of M1I+M6A gates. The extra peak at 2.08 ppm in this case may reflect intermolecular interactions involving Gly-rich and M1I+M6A rings on separate molecules, discussed above. The absence of *in* state peaks in Fig. 4*D* provides further evidence for the absence of allostery between the two gated ends, as the presence of a WT distribution of gates at the distal end does not lead to any change in the positioning of the Gly gates, which remain in the all-*out* configuration.

L81V Mutation as a Probe of 20S CP Allostery. The 11S RP binding and the gate mutation studies described above provide strong evidence that the gating equilibrium at one end of the 20S CP is not influenced by the corresponding equilibrium at the opposite end of the molecule. This suggests that the allosteric pathway that extends between the two proximal α_7-β_7 rings on the same half of the proteasome, connecting sites of RP binding on one α_7-ring with active sites on the neighboring β_7 (47), does not continue further. As a further test, we have constructed a pair of asymmetric proteasomes where one face is "capped" by either S95C or L81V+S95C α_7-rings, neither of which are NMR active, with the other end containing an ILVM-$^{13}CH_3$ α_7-ring that is M1I+M6A+S95C (Fig. 5*A*, structures framed in green and gray). An additional 20S CP sample was generated where both α_7-rings are NMR active and contain the L81V substitution, as a control (Fig. 5*A*, red frame). We have shown previously that substitution of Val for Leu at position 81 of the α-subunit in symmetric CPs creates a set of CSPs that is very similar to that obtained from 11S RP binding to CPs with WT α_7-rings (47). These CSPs can also be recapitulated by mutations of the catalytic T1 residues in β_7-rings or through association of the small-molecule chloroquine, a low-affinity allosteric inhibitor (49) that binds at the interface between α- and β-subunits (47). Thus, the L81V mutation triggers the same "pathway" that 11S binding does (highlighted in Fig. 1*B*). If CSPs are observed in datasets recorded on the asymmetric construct of Fig. 5*A* (gray frame) that are similar to those noted in spectra of the symmetric α-L81V CP (red frame), then this would provide evidence of an extensive allosteric pathway spanning the full length of the 20S CP. In contrast, if spectra recorded on the pair of asymmetric CPs highlighted in Fig. 5*A* (green and gray frames) are superimposable, then this would strongly suggest that the allosteric path is confined to half of the proteasome.

Fig. 5*B* shows a number of panels highlighting selected regions of ^{13}C–^1H HMQC datasets recorded of CPs where each of the α_7-rings harbors the L81V mutation (red contours), or asymmetric CPs where one of the α_7-rings is M1I+M6A+S95C (ILVM-$^{13}CH_3$) and the other is either S95C (green) or L81V+S95C (gray). A number of methyl groups that show CSPs in comparisons of spectra of symmetric α-L81 and α-L81V CPs are selected and their positions in the proteasome structure illustrated in Fig. 5*C*. In all cases, the green and gray cross-peaks overlap and are distinct from the red correlations (Fig. 5*B* and *SI Appendix*, Fig. S5), indicating that the CSPs introduced at one α_7-ring by the L81V mutation do not extend to the second ring that is WT at position 81. These results provide further support that the allosteric pathway in the 20S CP is limited to adjacent α_7–β_7-rings.

Concluding Remarks. In a series of previous papers, we have shown that the *T. acidophilum* 20S CP proteasome is a dynamic molecular machine (19, 47, 58). Flexible gates control, in part, substrate entry into the lumen of the CP antechamber through stochastic fluctuations that place gating residues either *in* or *out* of the proteasome lumen (19). Proteasome function is further modulated through pathways of communication between distal parts of the molecule that can be manipulated through mutation, binding of RPs or inhibitors (45–48). For example, it was shown that one such pathway connects the proteasome gates with active-site residues located 70 Å away (47). Although high-resolution structures are increasingly forthcoming of proteasomes bound with a variety of different RPs (30, 32, 60), key questions relating to the roles that dynamics and allostery might play in regulating function have remained. The development of NMR-based approaches to study high–molecular-weight particles through methyl-TROSY–based pulse schemes (54, 55), and the ability to asymmetrically label molecules so as to probe how perturbations in one region affect the structure and dynamics at a distal location (21, 61), opens up the possibilities for an in-depth analysis of the structure–dynamics–function paradigm in this important class of molecule and, indeed, in a range of large protein complexes. In particular, these advances allow us to explore here the range of allosteric communication in the proteasome system. Our results establish that, although extensive, the allosteric pathway that couples RP binding sites on the α_7-ring to catalytic T1 residues of the β_7-ring does not extend further with perturbations to the CP, such as binding of the

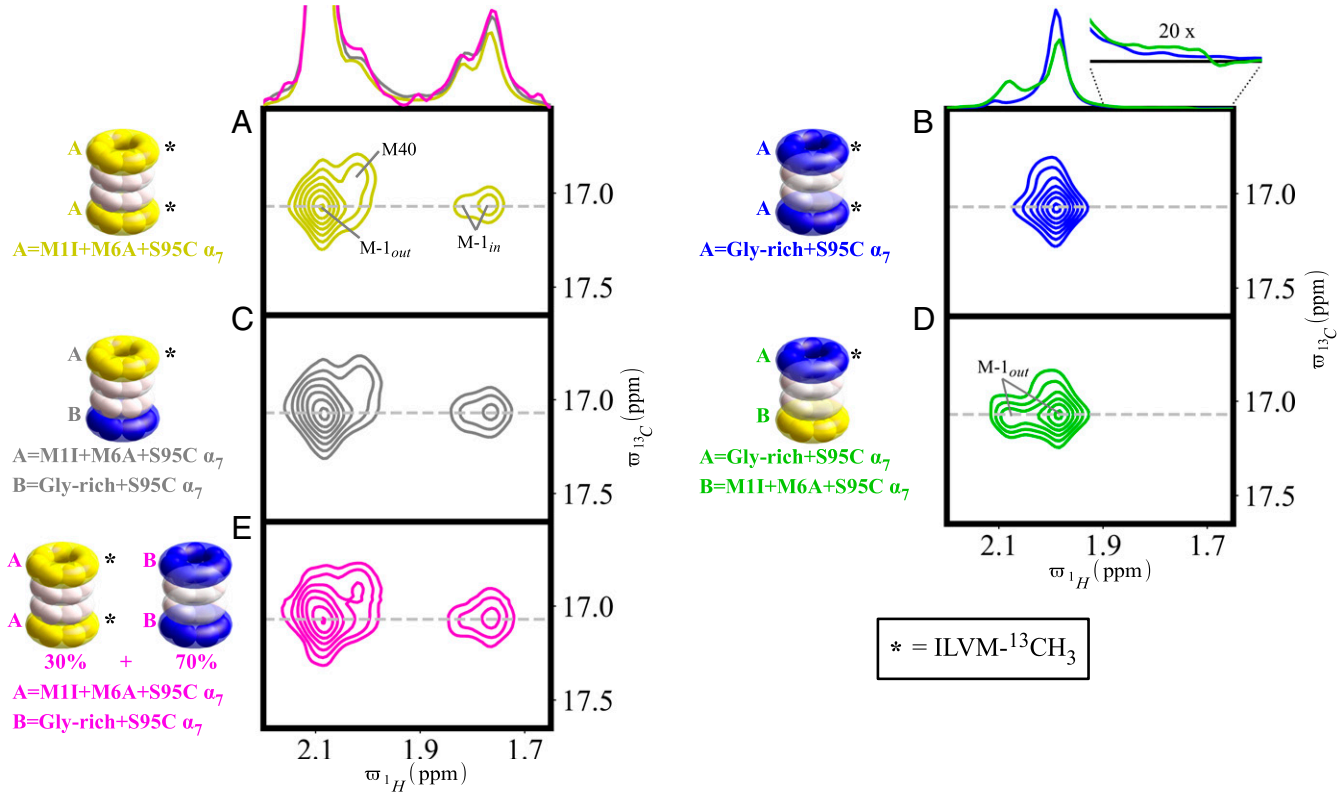

Fig. 4. Testing long-range allostery in the 20S CP through gate mutation. (*A–E*) Spectral regions highlighting correlations from M-1_{out} and M-1_{in} are shown, along with traces (gray dashed lines) indicated above each of the set of plots. (*A* and *B*) Symmetric 20S CPs were generated where both α_7-rings are NMR active and contain either M1I+M6A+S95C (*A*) or Gly-rich+S95C (*B*) α-protomers, as controls. (*C* and *D*) A pair of asymmetric CPs has been prepared, containing Gly-rich+S95C (blue) and M1I+M6A+S95C (yellow) α_7-rings at opposite ends of the molecule. One of the two α_7-rings is ILVM-$^{13}CH_3$ labeled, as indicated with an asterisk (*). (*E*) A last control sample contained a mixture of a pair of symmetric 20S CPs, one with ILVM-$^{13}CH_3$ M1I+M6A+S95C α_7-rings and a second composed of unlabeled Gly-rich+S95C α_7-rings in the ratio 3:7. See text for further details.

11S RP, nor by drastically changing the gating equilibrium on one side of the CP or by modification of the pathway via mutation. The physical basis for why the allosteric pathway extends for only half of the proteasome is not currently understood. A previous NMR study establishes that, while the chemical shift changes that accompany proteasome perturbations have enabled delineation of an allosteric pathway, the changes to the overall structure are subtle, likely involving slight rotations about the interfaces between adjacent protomers (47). Notably, in a very recent combined biochemical, cryoelectron microscopy study that has appeared in bioRxiv, Cheng and coworkers (62) demonstrate that binding of the WT 11S RP at one end of the proteasome has no effect on gating at the opposite side, in agreement with our findings. However, when a modified 11S is used that substitutes the final eight C-terminal residues for those in the PAN activator that includes a HbYX (hydrophobic, tyrosine, any residue) motif, or when PAN itself is used, opening of the gate at one end leads to a similar opening 150 Å removed. It therefore appears that binding-induced gating cooperativity depends on the interacting RP and whether or not it contains a HbYX motif. The exact mechanism is not clear, but rotation of the α-subunits in the ring to which activator is bound is thought to be critical (62). Interestingly, however, rotation of the α-subunits in the distal ring that is not bound to the HbYX-containing activator does not seem to occur, suggesting that a distinction between RP-bound and -unbound halves of the proteasome still remains and that binding of a RP at one end cannot enforce some of the same structural changes at the other side.

Our work establishes that the allosteric network that we observed previously and that could be manipulated through point mutations at key residues or by the binding of the 11S RP does not extend beyond one-half of the proteasome. The fact that this pathway is limited may be significant. Biochemical experiments have established that, at least in eukaryotic cells, "hybrid" proteasomes exist, consisting of different RPs, such as the ATP-dependent 19S (PA700) and the ATP-independent 11S (PA28), on opposite ends of the molecule (63–65). These complexes were estimated to

Table 3. Populations of *in* gates in 20S CPs containing Gly-rich α_7-rings

20S CP type	Gate type	*In*
Symmetric	ILVM-$^{13}CH_3$ M1I+M6A+S95C	28.8 ± 0.6%
	ILVM-$^{13}CH_3$ Gly-rich+S95C	<2%
Asymmetric	ILVM-$^{13}CH_3$ M1I+M6A+S95C/unlabeled Gly-rich+S95C	35.0 ± 0.5%
	ILVM-$^{13}CH_3$ Gly-rich+S95C/unlabeled M1I+M6A+S95C	<2%
Mixture of symmetric CPs	30% ILVM-$^{13}CH_3$ M1I+M6A+S95C + 70% unlabeled Gly-rich+S95C	34.9 ± 0.8%

Observed populations are calculated from peak volumes, corrected for differential transverse relaxation.

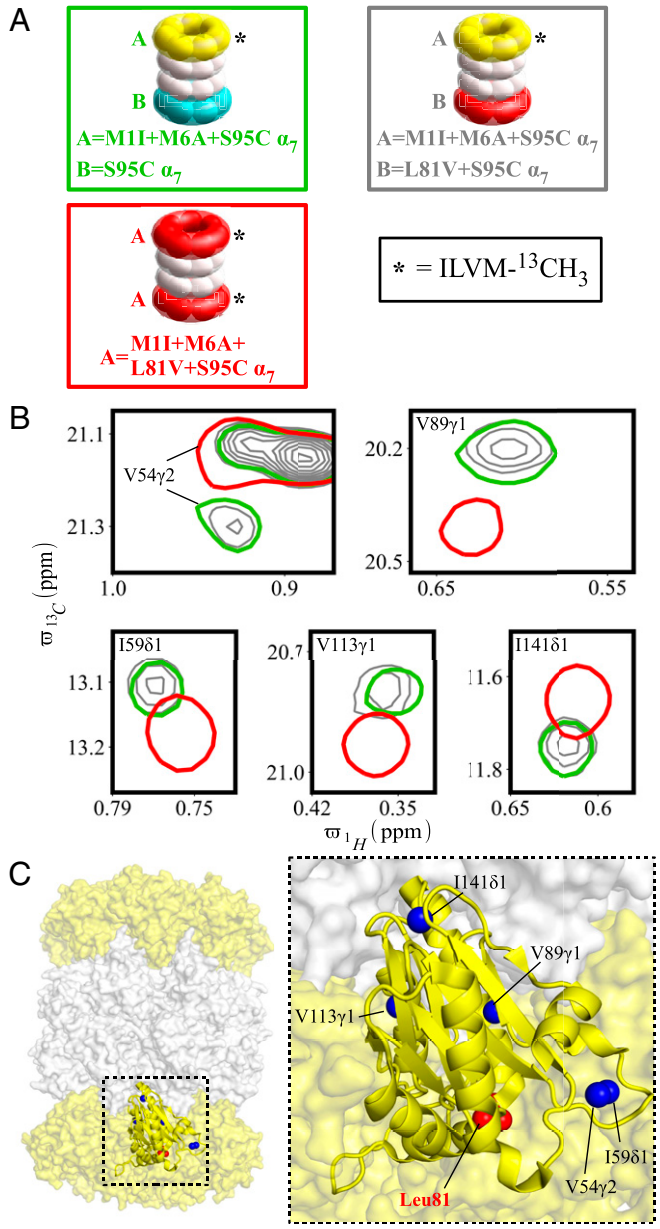

Fig. 5. Testing long-range allostery in the 20S CP via L81V mutations. (*A*) A pair of asymmetric proteasomes has been prepared, containing either an S95C (green frame) or an L81V+S95C (gray frame) α_7-ring that is not NMR active at one end, and an ILVM-$^{13}CH_3$ M1I+M6A+S95C α_7-ring at the other end (*). An additional 20S CP (symmetric) was generated where both α_7-rings are NMR active (*) and contain the L81V substitution (red frame), as a control. (*B*) Spectral regions of a ^{13}C–^{1}H HMQC dataset containing selected peaks derived from residues that are part of the allosteric pathway linking the α-subunits with the βT1 active sites. Shown with red, gray, and green contours are correlations derived from M1I+M6A+L81V+S95C symmetric (construct in red frame), M1I+M6A+S95C/L81V+S95C asymmetric (gray frame), and M1I+M6A+S95C/S95C asymmetric (green frame) CPs. The positions of these residues are indicated in the expanded structure shown in *C*, *Right*, by the blue spheres, with the red spheres denoting side-chain atoms of the mutated L81 residue. Surrounding α- and β-subunits are shown as yellow and white surfaces, respectively, as highlighted in the full structure on the *Left*.

account for about 25% of all proteasomes in extracts from HeLa cells and were found to be up-regulated by IFN-γ[64], a cytokine that modulates the immune system (66). Notably, the different RPs that are bound to hybrid proteasomes have different biological roles. For example, the 11S RP stimulates the release of peptide products that, in turn, play a role in the immune system (39, 40, 67–69), while the 19S RP recognizes ubiquitinated substrates and feeds them into the CP for degradation (9, 23, 24). While binding of an 11S RP can stimulate a path in the proteasome-half with which it interacts, restricting the extent of the resulting structural changes to a single α_7–β_7 unit in some cases may increase the functionality of the CP by allowing it to be responsive to separate RPs in the case where they are bound simultaneously. Alternatively, in cases where only one end of the CP is capped by an 11S RP, maintaining a closed gating conformation at the second side may play a role in ensuring that indiscriminate degradation of substrates does not occur.

Materials and Methods

Protein Production. The 11S RP from *Trypanosoma brucei* (perdeuterated) (44) was expressed with an N-terminal His_6-TEV sequence, *T. acidophilum* 20S CP β subunits (unlabeled) were expressed with an N-terminal NusA-His_6-TEV sequence, and *T. acidophilum* ILVM-$^{13}CH_3$–labeled α-subunits included an N-terminal His_6-SUMO sequence. Finally, a His_6-SUMO-Strep-tag II-TEV sequence was added to the N terminus of α-subunits for expression in unlabeled media [Strep-tag II = Trp-Ser-His-Pro-Gln-Phe-Glu-Lys (56)]. Protein expression was carried out using BL21 (DE3) *Escherichia coli* cells.

All unlabeled proteins were expressed in LB broth using an incubator shaker, expect for the β-subunits where expression was performed using TB broth via a single 10-L growth in a fermenter to maximize yield. Perdeuterated 11S and ILVM-$^{13}CH_3$–labeled α-subunits were expressed in M9 minimal media, 99% D_2O, with d_7-glucose as the sole carbon source. For selective ILVM methyl labeling, 100 mg/L [ε-^{13}C]-methionine (CLM-206-PK; Cambridge Isotope Laboratories), 60 mg/L α-ketobutyric acid (CDLM-7318; Cambridge Isotope Laboratories), and 100 mg/L α-ketoisovaleric acid (CDLM-7317; Cambridge Isotope Laboratories; one of the two isopropyl methyl groups is $^{13}CH_3$, the second is $^{12}CD_3$) were added 1 h before the induction of protein overexpression (52, 53). Cells were grown at 37 °C until OD ∼ 0.8, and then induced using 0.25 mM IPTG with overnight protein expression at room temperature. Cells resuspended in 50 mM sodium phosphate buffer, pH 7.8, 0.5 M NaCl, were lysed by sonication in the presence of DNase I and protease inhibitors, and the soluble cellular fraction was passed through a HisTrap column (GE Healthcare) and subsequently eluted with 0.3 M imidazole in 100 mM sodium phosphate buffer, pH 7.8. The N-terminal tags were then cleaved either with TEV protease (11S, β-subunit) or with UlP1 protease (α-subunit) and the protein passed again through the HisTrap column, collecting the flow-through. The final purification step involved size-exclusion chromatography with a Superdex 200 column (11S, α-subunit) in 50 mM sodium phosphate buffer, pH 7.8, 100 mM NaCl or anion exchange chromatography (β-subunit) using a HiTrap Q column (GE Healthcare) in Tris·HCl buffer, pH 8, and a NaCl gradient between 0 and 0.6 M.

Production of Asymmetric 20S Core Particles. ILVM-$^{13}CH_3$–labeled α-subunits, unlabeled α-subunits with an N-terminal Strep-tag II-TEV sequence, and unlabeled β-subunits were mixed at a 1:1:≥2 ratio, respectively; the β-subunit was added in excess of the strictly required 1:1:2 ratio to increase the yield of 20S CPs that were produced. Since equal amounts of the two starting α-subunits were used, it is expected that 20S CPs will be produced where 50% are asymmetric (α_{7ILVM}-β_7-β_7-α_7; note that mutations are added to the labeled or unlabeled α_7-rings, depending on the experiment, as described in the text), 25% are symmetric and unlabeled, and the last quarter is symmetric with both α_7-rings ILVM-$^{13}CH_3$ labeled (see schematic of Fig. 1*F*). The concentration of each of the two types of α-rings (labeled and unlabeled) was ∼1 to 2 μM in a volume of about 70 mL, and incubation occurred overnight at 37 °C. The mixture was passed through a 1.0-μm filter and concentrated at 4 °C in Amicon Ultra-15 centrifugal filter units with 100-kDa cutoffs before injection on a Superdex 200 size-exclusion column equilibrated in 50 mM sodium phosphate buffer, pH 7.8, 100 mM NaCl. Size-exclusion chromatography was repeated at least a second time to minimize residual α_7-rings in the 20S CP fraction. Purified 20S CPs were then passed through a Strep-Tactin column (StrepTrap HP; GE Healthcare), and the eluant collected upon addition of 2.5 mM desthiobiotin. The N-terminal Strep-tag II was then cleaved with TEV protease and the sample passed again through the Strep-Tactin column, collecting the flow-through. This procedure generates two types of 20S CPs for NMR, including the desired asymmetric particles where one of the two α_7-rings is ILVM-$^{13}CH_3$ labeled, as well as symmetric particles that are not NMR labeled and hence invisible in experiments.

The quantities of protein in the flow-through and eluted fractions from the Strep-Tactin column were quantified by absorbance at 280 nm (Fig. 1*F*).

Notably, although 25% of the total protein was expected in the flow-through (*f.t.*), a higher proportion was observed, the result of proteasomal degradation of all seven Strep-tags in some of the α_7-rings. The fraction of desired asymmetric 20S CPs in the NMR sample (i.e., in the eluted fraction), $p(asymmetric)$, can be calculated as follows: Let the fraction of protein in the *f.t.* be $p(f.t.)$. Then, $p(f.t.) = 0.25 + 0.25f^2 + 0.5f$, where f is the probability that all Strep-tags in an α_7-ring are degraded. Note that the second term derives from CPs where both α_7-rings were originally Strep-tagged, while the third term corresponds to CPs where one of the rings was originally tagged, and in both cases all of the tags were cleaved by proteasomes during the purification process. The value f can be calculated to be $f = -1 + 2\sqrt{p(f.t.)}$, from which the fraction of total eluted protein (i.e., not in flow-through) can be obtained, as $0.25(1 - f^2) + 0.5(1 - f)$. Thus, $p(asymmetric) = 0.5(1 - f)/\{0.25(1 - f^2) + 0.5(1 - f)\}$, so that $p(asymmetric) = (1 - \sqrt{p(f.t.)})/(1 - p(f.t.))$. Note that in the absence of degradation of the Strep-tag, $p(f.t.) = 25\%$ and $p(asymmetric) = 66.7\%$. In the limit of complete degradation it can be calculated that

$$\lim_{p(f.t.)\to 1} p(asymmetric) = \lim_{p(f.t.)\to 1} \frac{1-\sqrt{p(f.t.)}}{1-p(f.t.)} = \lim_{p(f.t.)\to 1} \frac{-1\Big/\left(2\cdot\sqrt{p(f.t.)}\right)}{-1} = 50\%.$$

As the change in $p(asymmetric)$ is small, from 50 to 66.7%, as $p(f.t.)$ varies from 100 to 25%, any error in $p(f.t.)$ (estimated to be less than 5%) translates into a small uncertainty in the calculated $p(asymmetric)$ value (less than 1%).

NMR Experiments. NMR experiments were performed on Bruker Avance III HD 14.1 T (all of the experiments with single α_7-rings; Fig. 2) or 18.8 T (all of the experiments with 20S CPs; Figs. 3–5) spectrometers equipped with cryogenically cooled, *x,y,z* pulsed-field gradient triple-resonance probes. ^{13}C–^{1}H HMQC experiments were recorded on ILVM-$^{13}CH_3$–labeled proteins dissolved in D_2O buffer containing 25 mM potassium phosphate, pH 7.5, 50 mM NaCl, 0.03% sodium azide, and 1 mM EDTA. All NMR experiments with the 11S RP were acquired at 40 °C, while the other datasets recorded of the isolated 20S CP (those in Figs. 4 and 5*B* and *SI Appendix*, Figs. S4 and S5) were measured at 60 °C. In order to obtain robust estimates of fractional populations of states from their corresponding peak intensities, it is important to correct for differential magnetization losses from ^{1}H transverse relaxation during transfer times from ^{1}H to ^{13}C and back in HMQC experiments. ^{1}H R_2 rates of the *in* and *out* resonances (M-1) were measured using a modified 2D ^{13}C–^{1}H HMQC experiment, which included a chemical shift and scalar coupling refocused relaxation delay immediately prior to recording ^{1}H magnetization (t_2), as described previously (21, 57).

Estimation of Fractional Populations of States. Peak volumes were obtained by integration over boxes using the nmrDraw (70) suite of programs for data analysis. Volumes were adjusted to account for different ^{1}H R_2 rates by multiplication with the factor $\exp(R_2 \cdot 0.0072)$ (21), where 7.2 ms is the total constant-time evolution of ^{1}H magnetization during which it dephases and then rephases from the one bond ^{1}H–^{13}C scalar coupling. R_2 values for the peaks derived from the two *in*, one *out*, and one *tethered* conformations of M-1 in the individual α_7-rings, measured at 14.1 T (40 °C), are 36.5 ± 1.1, 28.9 ± 3.2, 6.79 ± 0.13, and 31.5 ± 0.5 s^{-1}, respectively. ^{1}H R_2 rates, measured at 18.8 T (40 °C), for the corresponding peaks of α–M-1 in the 20S CP are 70.8 ± 2.4, 61.1 ± 1.5, 10.40 ± 0.06, and 62.4 ± 1.7 s^{-1}, respectively. Finally, ^{1}H R_2 rates, measured at 18.8 T (60 °C), for the two *in* peaks and one *out* peak of α–M-1 for M1I+M6A+S95C gates in the 20S CP are 41.2 ± 2.9, 42.6 ± 1.6 and 9.5 ± 0.2 s^{-1}, respectively, while ^{1}H R_2 rates for the two *out* peaks of α–M-1 for the Gly-rich gates in the 20S CP are 12.4 ± 0.2 and 16.1 ± 0.6 s^{-1}.

Calculation of Fractional Populations of Five States of Fig. 2*B*.
M1I+M6A+S95C single α_7-ring + 11S. Total concentrations of α_7-rings ($[\alpha_7]_T$) and 11S particles ($[11S]_T$) were $[\alpha_7]_T$ = 13.6 μM and $[11S]_T$ = 40.7 μM, respectively (1:3). Values for $p(in) = p(\mathbf{A}) + p(\mathbf{C})$, $p(out) = p(\mathbf{B}) + p(\mathbf{D})$, and $p(tet) = p(\mathbf{E})$, corrected for differential ^{1}H relaxation (see above), are listed in Table 1 (Fig. 2 *B* and *C*). From the extracted, corrected volumes, it follows that $p(\mathbf{A}) + p(\mathbf{C}) = 12.0 \pm 0.8\%$, $p(\mathbf{B}) + p(\mathbf{D}) = 24.4 \pm 4.0\%$, and $p(\mathbf{E}) = 63.6 \pm 4.5\%$. The relative volumes of the L81δ1 peaks that report on 11S bound and free α_7-rings in this case provide an additional constraint, $p(\mathbf{C}) + p(\mathbf{D}) + p(\mathbf{E}) = 89 \pm 3\%$. Finally, $p(\mathbf{A})$ is set to $0.4 \cdot p(\mathbf{B})$, as both the present and previous studies (19, 21, 47) have shown that two of seven gates are localized to the *in* position. These five equations can be solved to yield the $p(\mathbf{J})$ values listed in the text and the values of $p(\mathbf{J})$ along with $[11S]_T$ and $[\alpha_7]_T$ used to calculate $K_D^I = ([\mathbf{A}] + [\mathbf{B}]) \cdot [\mathbf{L}]/([\mathbf{C}] + [\mathbf{D}] + [\mathbf{E}]) = 3.5 \pm 1.2$ μM. Values for the conditional probabilities $p(in|I^{BD}) = p(\mathbf{C})/[p(\mathbf{C}) + p(\mathbf{D}) + P(\mathbf{E})]$, $p(out|I^{BD}) = p(\mathbf{D})/[p(\mathbf{C}) + p(\mathbf{D}) + P(\mathbf{E})]$, and $p(tet|I^{BD}) = p(\mathbf{E})/[p(\mathbf{C}) + p(\mathbf{D}) + P(\mathbf{E})]$ are calculated to be 10.0 ± 2.0%, 18.5 ± 4.1%, and 71.5 ± 5.4%, respectively.
M1I+M6A+K66A+S95C single α_7-ring + 11S. All concentrations are as for *M1I+M6A+S95C single α7-ring + 11S* above. From the relaxation corrected cross-peak volumes it follows that $p(\mathbf{A}) + p(\mathbf{C}) = 23.2 \pm 1.7\%$, $p(\mathbf{B}) + p(\mathbf{D}) = 57.7 \pm 2.4\%$, and $p(\mathbf{E}) = 19.2 \pm 1.1\%$; $p(\mathbf{A})$ is set to $0.4 \cdot p(\mathbf{B})$. The absence of a L81δ1 peak for the 11S bound state implies that binding is somewhat different from for the K66 α_7-ring, as expected since a stabilizing salt bridge that is normally formed between each K66 of the seven α-ring protomers and the C-terminal residue of each of the seven subunits of the 11S RP is now absent (Fig. 2*E*). The second prong of the interaction, involving the so-called 11S activation loop (42), is still present. We distinguish the higher-affinity interaction involving both prongs and the lower-affinity interaction involving only the activation loop by I and II, respectively. The system of equations listed above are underdetermined. We assume, therefore, that $p(tet|II^{BD}) = p(tet|I^{BD})$, from which the values of $p(\mathbf{J})$ reported in the text are obtained. $K_D^{II} = ([\mathbf{A}] + [\mathbf{B}]) \cdot [\mathbf{L}]/([\mathbf{C}] + [\mathbf{D}] + [\mathbf{E}])$ is calculated to be 101 ± 14 μM.

Distinguishing between Models of Complete and No Cooperativity via 11S Binding Experiments. NMR samples of the 20S CP have been prepared as described above, containing symmetric CPs (M1I+M6A+S95C α_7-rings, NMR invisible) and asymmetric (1 NMR-active M1I+M6A+K66A+S95C α_7-ring + 1 NMR-inactive M1I+M6A+S95C α_7-ring) CPs (Fig. 3*A*). Concentrations of the 20S CP and of the 11S RP are 22.4 and 64.6 μM, respectively, and since 46% of the CPs were symmetric, the total concentration of K66 α_7-rings (high affinity, I) is $[P_I]_T = 22.4\ \mu M \cdot 0.46 \cdot 2 + 22.4\ \mu M \cdot 0.54 \cdot 1 = 32.7\ \mu M$ and, similarly, the concentration of K66A rings is $[P_{II}]_T = 12.1$ μM. The relative fractions of bound K66 α_7-rings $p(I^{BD})$ and of bound K66A α_7-rings $p(II^{BD})$ can be calculated from the simultaneous equilibria,

$$P_I + L \overset{K_D^I}{\rightleftharpoons} P_IL,\ P_I = \text{K66 } \alpha_7\text{-rings}$$
$$P_{II} + L \overset{K_D^{II}}{\rightleftharpoons} P_{II}L,\ P_{II} = \text{K66A } \alpha_7\text{-rings}.$$

It can be shown that

$$[L]^3 + ([P_I]_T - \alpha + K_D^I)[L]^2 + ([P_I]_T \cdot K_D^{II} - \beta - K_D^I \cdot \alpha) \cdot [L] - K_D^I \cdot \beta = 0$$
$$\alpha = [L]_T - K_D^{II} - [P_{II}]_T$$
$$\beta = [L]_T \cdot K_D^{II}$$
$$[P_IL] = \frac{[P_I]_T \cdot [L]}{K_D^I + [L]}$$
$$[P_{II}L] = \frac{[P_{II}]_T \cdot [L]}{K_D^{II} + [L]},$$

from which $p(I^{BD}) = [P_IL]/[P_I]_T$ and $p(II^{BD}) = [P_{II}L]/[P_{II}]_T$ can be calculated (0.90 ± 0.03 and 0.24 ± 0.03, respectively).

Data Availability Statement. All data discussed in the paper will be made available to readers upon request.

ACKNOWLEDGMENTS. This work was supported by grants from the Canadian Institutes of Health Research and the Natural Sciences and Engineering Research Council of Canada. L.E.K. holds a Canada Research Chair in Biochemistry. We thank Dr. Jacob P. Brady for help with using the fermenter for expression of the β-subunits of the 20S CP, and Drs. Algirdas Velyvis and Yifan Cheng (University of California, San Francisco) for useful discussions.

1. W. Baumeister, J. Walz, F. Zühl, E. Seemüller, The proteasome: Paradigm of a self-compartmentalizing protease. *Cell* **92**, 367–380 (1998).
2. A. L. Goldberg, Protein degradation and protection against misfolded or damaged proteins. *Nature* **426**, 895–899 (2003).
3. C. M. Pickart, R. E. Cohen, Proteasomes and their kin: Proteases in the machine age. *Nat. Rev. Mol. Cell Biol.* **5**, 177–187 (2004).
4. S. Bhattacharyya, H. Yu, C. Mim, A. Matouschek, Regulated protein turnover: Snapshots of the proteasome in action. *Nat. Rev. Mol. Cell Biol.* **15**, 122–133 (2014).
5. R. S. Marshall, R. D. Vierstra, Dynamic regulation of the 26S proteasome: From synthesis to degradation. *Front. Mol. Biosci.* **6**, 40 (2019).
6. B. Coll-Martínez, B. Crosas, How the 26S proteasome degrades ubiquitinated proteins in the cell. *Biomolecules* **9**, E395 (2019).
7. M. Chu-Ping, J. H. Vu, R. J. Proske, C. A. Slaughter, G. N. DeMartino, Identification, purification, and characterization of a high molecular weight, ATP-dependent activator (PA700) of the 20S proteasome. *J. Biol. Chem.* **269**, 3539–3547 (1994).

8. J. M. Peters, W. W. Franke, J. A. Kleinschmidt, Distinct 19S and 20S subcomplexes of the 26S proteasome and their distribution in the nucleus and the cytoplasm. *J. Biol. Chem.* **269**, 7709–7718 (1994).
9. C. W. Liu, A. D. Jacobson, Functions of the 19S complex in proteasomal degradation. *Trends Biochem. Sci.* **38**, 103–110 (2013).
10. J. M. Peters, Z. Cejka, J. R. Harris, J. A. Kleinschmidt, W. Baumeister, Structural features of the 26S proteasome complex. *J. Mol. Biol.* **234**, 932–937 (1993).
11. F. Kopp, L. Kuehn, Orientation of the 19S regulator relative to the 20S core proteasome: An immunoelectron microscopic study. *J. Mol. Biol.* **329**, 9–14 (2003).
12. W. Heinemeyer, N. Tröndle, G. Albrecht, D. H. Wolf, PRE5 and PRE6, the last missing genes encoding 20S proteasome subunits from yeast? Indication for a set of 14 different subunits in the eukaryotic proteasome core. *Biochemistry* **33**, 12229–12237 (1994).
13. M. Groll *et al*., Structure of 20S proteasome from yeast at 2.4 Å resolution. *Nature* **386**, 463–471 (1997).
14. M. Unno *et al*., The structure of the mammalian 20S proteasome at 2.75 Å resolution. *Structure* **10**, 609–618 (2002).
15. B. Dahlmann *et al*., The multicatalytic proteinase (prosome) is ubiquitous from eukaryotes to archaebacteria. *FEBS Lett.* **251**, 125–131 (1989).
16. P. Zwickl *et al*., Primary structure of the *Thermoplasma* proteasome and its implications for the structure, function, and evolution of the multicatalytic proteinase. *Biochemistry* **31**, 964–972 (1992).
17. J. Löwe *et al*., Crystal structure of the 20S proteasome from the archaeon *T. acidophilum* at 3.4 Å resolution. *Science* **268**, 533–539 (1995).
18. D. Finley, X. Chen, K. J. Walters, Gates, channels, and switches: Elements of the proteasome machine. *Trends Biochem. Sci.* **41**, 77–93 (2016).
19. T. L. Religa, R. Sprangers, L. E. Kay, Dynamic regulation of archaeal proteasome gate opening as studied by TROSY NMR. *Science* **328**, 98–102 (2010).
20. M. Groll *et al*., A gated channel into the proteasome core particle. *Nat. Struct. Biol.* **7**, 1062–1067 (2000).
21. R. Huang, F. Pérez, L. E. Kay, Probing the cooperativity of *Thermoplasma acidophilum* proteasome core particle gating by NMR spectroscopy. *Proc. Natl. Acad. Sci. U.S.A.* **114**, E9846–E9854 (2017).
22. A. J. Baldwin, T. L. Religa, D. F. Hansen, G. Bouvignies, L. E. Kay, $^{13}CHD_2$ methyl group probes of millisecond time scale exchange in proteins by ^{1}H relaxation dispersion: An application to proteasome gating residue dynamics. *J. Am. Chem. Soc.* **132**, 10992–10995 (2010).
23. Q. Deveraux, V. Ustrell, C. Pickart, M. Rechsteiner, A 26S protease subunit that binds ubiquitin conjugates. *J. Biol. Chem.* **269**, 7059–7061 (1994).
24. P. Young, Q. Deveraux, R. E. Beal, C. M. Pickart, M. Rechsteiner, Characterization of two polyubiquitin binding sites in the 26S protease subunit 5a. *J. Biol. Chem.* **273**, 5461–5467 (1998).
25. X. Huang, B. Luan, J. Wu, Y. Shi, An atomic structure of the human 26S proteasome. *Nat. Struct. Mol. Biol.* **23**, 778–785 (2016).
26. A. Schweitzer *et al*., Structure of the human 26S proteasome at a resolution of 3.9 Å. *Proc. Natl. Acad. Sci. U.S.A.* **113**, 7816–7821 (2016).
27. N. Benaroudj, E. Tarcsa, P. Cascio, A. L. Goldberg, The unfolding of substrates and ubiquitin-independent protein degradation by proteasomes. *Biochimie* **83**, 311–318 (2001).
28. D. Forouzan *et al*., The archaeal proteasome is regulated by a network of AAA ATPases. *J. Biol. Chem.* **287**, 39254–39262 (2012).
29. D. Barthelme, J. Z. Chen, J. Grabenstatter, T. A. Baker, R. T. Sauer, Architecture and assembly of the archaeal Cdc48*20S proteasome. *Proc. Natl. Acad. Sci. U.S.A.* **111**, E1687–E1694 (2014).
30. P. Majumder *et al*., Cryo-EM structures of the archaeal PAN-proteasome reveal an around-the-ring ATPase cycle. *Proc. Natl. Acad. Sci. U.S.A.* **116**, 534–539 (2019).
31. V. Ustrell, L. Hoffman, G. Pratt, M. Rechsteiner, PA200, a nuclear proteasome activator involved in DNA repair. *EMBO J.* **21**, 3516–3525 (2002).
32. A. Toste Rêgo, P. C. A. da Fonseca, Characterization of fully recombinant human 20S and 20S-PA200 proteasome complexes. *Mol. Cell* **76**, 138–147.e5 (2019).
33. M. Schmidt *et al*., The HEAT repeat protein Blm10 regulates the yeast proteasome by capping the core particle. *Nat. Struct. Mol. Biol.* **12**, 294–303 (2005).
34. J. Iwanczyk *et al*., Structure of the Blm10-20 S proteasome complex by cryo-electron microscopy. Insights into the mechanism of activation of mature yeast proteasomes. *J. Mol. Biol.* **363**, 648–659 (2006).
35. K. Sadre-Bazzaz, F. G. Whitby, H. Robinson, T. Formosa, C. P. Hill, Structure of a Blm10 complex reveals common mechanisms for proteasome binding and gate opening. *Mol. Cell* **37**, 728–735 (2010).
36. M. Yukawa *et al*., Proteasome and its novel endogeneous activator in human platelets. *Biochem. Biophys. Res. Commun.* **178**, 256–262 (1991).
37. C. P. Ma, C. A. Slaughter, G. N. DeMartino, Identification, purification, and characterization of a protein activator (PA28) of the 20S proteasome (macropain). *J. Biol. Chem.* **267**, 10515–10523 (1992).
38. W. Dubiel, G. Pratt, K. Ferrell, M. Rechsteiner, Purification of an 11S regulator of the multicatalytic protease. *J. Biol. Chem.* **267**, 22369–22377 (1992).
39. B. Honoré, H. Leffers, P. Madsen, J. E. Celis, Interferon-gamma up-regulates a unique set of proteins in human keratinocytes. Molecular cloning and expression of the cDNA encoding the RGD-sequence-containing protein IGUP I-5111. *Eur. J. Biochem.* **218**, 421–430 (1993).
40. C. Realini, W. Dubiel, G. Pratt, K. Ferrell, M. Rechsteiner, Molecular cloning and expression of a gamma-interferon-inducible activator of the multicatalytic protease. *J. Biol. Chem.* **269**, 20727–20732 (1994).
41. W. Y. To, C. C. Wang, Identification and characterization of an activated 20S proteasome in *Trypanosoma brucei*. *FEBS Lett.* **404**, 253–262 (1997).
42. A. Förster, E. I. Masters, F. G. Whitby, H. Robinson, C. P. Hill, The 1.9 Å structure of a proteasome-11S activator complex and implications for proteasome-PAN/PA700 interactions. *Mol. Cell* **18**, 589–599 (2005).
43. F. G. Whitby *et al*., Structural basis for the activation of 20S proteasomes by 11S regulators. *Nature* **408**, 115–120 (2000).
44. Y. Yao *et al*., Structural and functional characterizations of the proteasome-activating protein PA26 from *Trypanosoma brucei*. *J. Biol. Chem.* **274**, 33921–33930 (1999).
45. J. Li *et al*., Lysine 188 substitutions convert the pattern of proteasome activation by REGgamma to that of REGs alpha and beta. *EMBO J.* **20**, 3359–3369 (2001).
46. P. A. Osmulski, M. Hochstrasser, M. Gaczynska, A tetrahedral transition state at the active sites of the 20S proteasome is coupled to opening of the alpha-ring channel. *Structure* **17**, 1137–1147 (2009).
47. A. M. Ruschak, L. E. Kay, Proteasome allostery as a population shift between interchanging conformers. *Proc. Natl. Acad. Sci. U.S.A.* **109**, E3454–E3462 (2012).
48. M. F. Kleijnen *et al*., Stability of the proteasome can be regulated allosterically through engagement of its proteolytic active sites. *Nat. Struct. Mol. Biol.* **14**, 1180–1188 (2007).
49. R. Sprangers *et al*., TROSY-based NMR evidence for a novel class of 20S proteasome inhibitors. *Biochemistry* **47**, 6727–6734 (2008).
50. K. L. Rock, I. A. York, T. Saric, A. L. Goldberg, Protein degradation and the generation of MHC class I-presented peptides. *Adv. Immunol.* **80**, 1–70 (2002).
51. D. M. Smith *et al*., Docking of the proteasomal ATPases' carboxyl termini in the 20S proteasome's alpha ring opens the gate for substrate entry. *Mol. Cell* **27**, 731–744 (2007).
52. V. Tugarinov, P. M. Hwang, L. E. Kay, Nuclear magnetic resonance spectroscopy of high-molecular-weight proteins. *Annu. Rev. Biochem.* **73**, 107–146 (2004).
53. V. Tugarinov, V. Kanelis, L. E. Kay, Isotope labeling strategies for the study of high-molecular-weight proteins by solution NMR spectroscopy. *Nat. Protoc.* **1**, 749–754 (2006).
54. V. Tugarinov, P. M. Hwang, J. E. Ollerenshaw, L. E. Kay, Cross-correlated relaxation enhanced ^{1}H–^{13}C NMR spectroscopy of methyl groups in very high molecular weight proteins and protein complexes. *J. Am. Chem. Soc.* **125**, 10420–10428 (2003).
55. R. Rosenzweig, L. E. Kay, Bringing dynamic molecular machines into focus by methyl-TROSY NMR. *Annu. Rev. Biochem.* **83**, 291–315 (2014).
56. T. G. Schmidt, J. Koepke, R. Frank, A. Skerra, Molecular interaction between the Strep-tag affinity peptide and its cognate target, streptavidin. *J. Mol. Biol.* **255**, 753–766 (1996).
57. M. P. Latham, A. Sekhar, L. E. Kay, Understanding the mechanism of proteasome 20S core particle gating. *Proc. Natl. Acad. Sci. U.S.A.* **111**, 5532–5537 (2014).
58. R. Sprangers, L. E. Kay, Quantitative dynamics and binding studies of the 20S proteasome by NMR. *Nature* **445**, 618–622 (2007).
59. Z. X. Wang, An exact mathematical expression for describing competitive binding of two different ligands to a protein molecule. *FEBS Lett.* **360**, 111–114 (1995).
60. S. C. Xie *et al*., The structure of the PA28-20S proteasome complex from Plasmodium falciparum and implications for proteostasis. *Nat. Microbiol.* **4**, 1990–2000 (2019).
61. R. Huang, Z. A. Ripstein, J. L. Rubinstein, L. E. Kay, Cooperative subunit dynamics modulate p97 function. *Proc. Natl. Acad. Sci. U.S.A.* **116**, 158–167 (2019).
62. Z. Yu *et al*., Allosteric coupling between α-rings of the 20S proteasome. bioRxiv:10.1101/832113 (7 November 2019).
63. K. B. Hendil, S. Khan, K. Tanaka, Simultaneous binding of PA28 and PA700 activators to 20 S proteasomes. *Biochem. J.* **332**, 749–754 (1998).
64. N. Tanahashi *et al*., Hybrid proteasomes. Induction by interferon-gamma and contribution to ATP-dependent proteolysis. *J. Biol. Chem.* **275**, 14336–14345 (2000).
65. P. Cascio, M. Call, B. M. Petre, T. Walz, A. L. Goldberg, Properties of the hybrid form of the 26S proteasome containing both 19S and PA28 complexes. *EMBO J.* **21**, 2636–2645 (2002).
66. K. Schroder, P. J. Hertzog, T. Ravasi, D. A. Hume, Interferon-gamma: An overview of signals, mechanisms and functions. *J. Leukoc. Biol.* **75**, 163–189 (2004).
67. Y. Sun *et al*., Expression of the proteasome activator PA28 rescues the presentation of a cytotoxic T lymphocyte epitope on melanoma cells. *Cancer Res.* **62**, 2875–2882 (2002).
68. J. Sun *et al*., The 11S proteasome subunit PSME3 is a positive feedforward regulator of NF-κB and important for host defense against bacterial pathogens. *Cell Rep.* **14**, 737–749 (2016).
69. K. Ahn *et al*., In vivo characterization of the proteasome regulator PA28. *J. Biol. Chem.* **271**, 18237–18242 (1996).
70. F. Delaglio *et al*., NMRPipe: A multidimensional spectral processing system based on UNIX pipes. *J. Biomol. NMR* **6**, 277–293 (1995).